Spring 2011

Shale gas rock characterization and 3D submicron pore network reconstruction

Malek Elgmati

Department:

SHALE GAS ROCK CHARACTERIZATION AND 3D SUBMICRON PORE NETWORK RECONSTRUCTION

by

MALEK ELGMATI

A THESIS

Presented to the Faculty of the Graduate School of the

MISSOURI UNIVERSITY OF SCIENCE AND TECHNOLOGY

In Partial Fulfillment of the Requirements for the Degree

MASTER OF SCIENCE IN PETROLEUM ENGINEERING

2011

Approved by

Baojun Bai, Advisor
Ralph Flori, Co-Advisor
Francisca Oboh-Ikuenobe
Andreas Eckert

ABSTRACT

Determining shale gas petrophysical properties is the cornerstone to any reservoir-management practice. Hitherto, conventional core analyses are inadequate to attain the petrophysical properties of shale gas at submicron-scale. This study combines interdisciplinary techniques from material science, petrophysics, and geochemistry to characterize different shale gas samples from North America including Utica, Haynesville and Fayetteville shale gas plays. Submicron pore structure, clay mineralogy, wettability and organic matter maturation were investigated to evaluate the petrophysical properties of shale gas rocks and to determine the impact of organic and inorganic matters on wettability alteration for different fracturing fluids on shale gas rocks.

High pressure (up to 60,000 psi) mercury porosimetry analysis (MICP) determined the pore size distributions. A robust detailed sequential milling and imaging procedure using dual beam (SEM/FIB) instrument was implemented successfully to characterize the submicron-pore structures. Various types of porosities were observed on SEM images. Pores were found in organic matters with the size of nano level and occupied 40−50% of the kerogen body. The reconstructed 3D pore model provided key insights into the petrophysical properties of shale gas such as pore size histogram, porosity, tortuosity and anisotropy, etc. X-ray diffraction (XRD) analysis showed high illite content in Haynesville shale. It also suggested high calcite content in Utica shale samples. Wettability tests showed that most of the additives that were used can alter shale gas surfaces toward hydrophilic-like system (water-wet). Moreover, palynofacies analysis provided valuable information about kerogen type and its degree of thermal maturation, which are key parameters in shale gas exploration.

ACKNOWLEDGMENTS

First and foremost, I praise Almighty God “Allah” for his blessings, grace and guidance. I would like to express my heartfelt gratitude to my parents who believed in me and encouraged me to take up higher studies.

I would like to express sincere thanks to my advisor, Dr. Baojun Bai for giving me an opportunity to conduct this research and for his support, guidance and patience throughout this project. I would also like to extend my appreciations to the members of my committee, Dr. Ralph Flori, Dr. Francisca Oboh-Ikuenobe and Dr. Andreas Eckert, for their constructive criticism, encouragement and insightful comments.

My particular gratitude is also extended to Dr. Kai Song, Elizabeth Ann Kulp, Hao Zhang, Dr. David J. Wronkiewicz and Alsedik Abousif for their contributions. A successful completion of this work would not have been possible without their help.

Special thanks also go to Dr. Timothy Kneafsey of Berkeley National Lab for his long-distance assistance and support.

I am heartily thankful to Mohamed Zobaa who assisted me in carrying out the palynofacies analysis. His interpretations have been the vital element of this study.

I also thank Mr. Doug Melton, Mr. Mike Engle from Southwest Energy and Dr. Qi Qu from Baker-Hughes Company for generosity in providing me with the shale gas samples.

Last but not least, my special thanks to the fellow graduate students, the faculty and the staff at the Geological Sciences and Engineering department for their help all through my Masters.

TABLE OF CONTENTS

LIST OF ILLUSTRATIONS

LIST OF TABLES

NOMENCLATURE

Symbol	Description
σ	Surface tension
p	Pressure
r	Pore throat radius
d_p	Pore throat diameter
k	Permeability
k_x	Permeability in x direction
k_y	Permeability in y direction
k_z	Permeability in z direction
k_v	Vertical permeability
k_h	Horizontal permeability
ϕ	Porosity
θ	Contact angle/Diffraction angle
τ	Tortuosity
L	Total sample length
L_a	Actual flow path length
β	Anisotropy
n	Integer
λ	Wavelength
d	Spacing
γ^{sl}	Solid-liquid interfacial tension
γ^{lv}	Liquid surface tension
γ^{sv}	Solid surface tension
h	Drop height
w	Drop width

1. INTRODUCTION

1.1. NATURAL GAS INDUSTRY IN THE UNITED STATES

Natural gas is a fossil fuel primarily made of methane, hydrogen and carbon. The importance of natural gas has increased steadily to become the vital component of the US energy supply. Natural gas is relatively safe and abundant for industrial use. According to the US Energy Information Administration (EIA), natural gas is more environmentally friendly and attractive compared to other energy resources due to its ecological advantages (low levels of carbon dioxide CO2 emission) and better safety qualities (insignificant sulfur dioxide contents, SO2%). Table 1.1 shows a comparison of the combustion emissions level for three sources of fossil fuel.

Table 1.1. Fossil Fuel Combustion Emissions
LB/Billion BTU (Source: EIA, 1998)

Air Pollutant	Combusted Source		
	Natural Gas	Oil	Coal
Carbon dioxide (CO_2)	117,000	164,000	208,000
Carbon monoxide (CO)	40	33	208
Nitrogen oxides (NO_x)	92	448	457
Sulfur dioxide (SO_2)	0.6	1,122	2,591
Particulates (PM)	7.0	84	2,744
Formaldehyde	0.750	0.220	0.221
Mercury (Hg)	0.000	0.007	0.016

Natural gas production was not actively pursued for long time. It is probably due to lack of the infrastructure of transportation and the proper technology to handle it. However, with expanding natural gas pipeline network, advent of specialized ships for

transporting natural gas as LNG, depleting oil reserves and constricting anti flaring regulations have made natural gas production attractive. Figure 1.1 shows more than 210 natural gas pipeline systems allocated between interstate and intrastate transmission pipelines and liquefied natural gas (LNG) facilities.

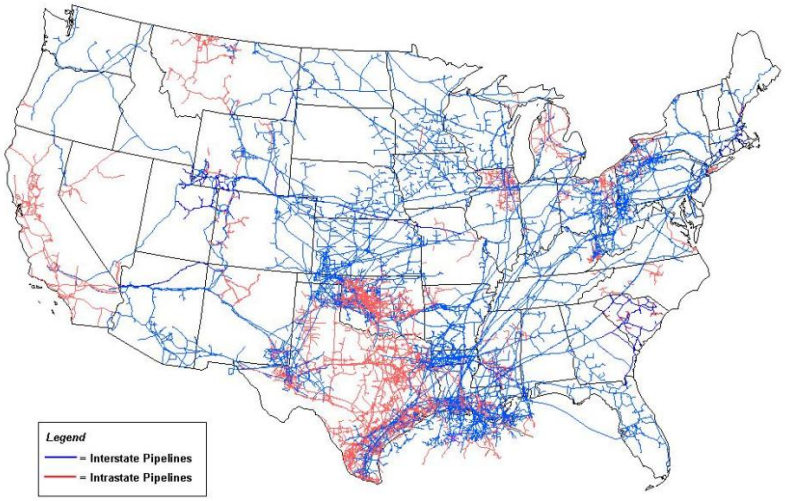

Figure 1.1. The US Natural Gas Pipeline Network Map
(Source: EIA, 2009)

The growth of natural gas reserves and production has sparked interest in the US natural gas resources. The United States is one of the largest producers of natural gas. According to the EIA annual energy outlook of 2011, the United States possesses 2,552 trillion cubic feet (Tcf) of potential natural gas resources. Natural gas from shale resources accounts for 827 Tcf of this resource estimate (i.e. 32.4% of the total natural gas reserve). This natural gas reserve is enough to supply approximately 110 years of use with the annual natural gas production of 23.3 Tcf (EIA, 2010). Shale gas annual production rate have increased significantly between the 2009 and 2011 from 3.28 to 5.11 Tcf and are likely to increase further in the future.

Natural gas finds extensive use in the residential and commercial applications, for power generation and as an alternative transportation fuel. According to the American Public Gas Association (APGA), natural gas currently supplies more than one-half of the energy consumed by residential and commercial customers, and about 41 percent of the energy used by U.S. industry. Moreover, 87% of the supplied natural gas in the United States was produced domestically (EIA, 2009). Thus, the supply of natural gas is not as dependent on foreign producers as is the supply of crude oil, and the delivery system is less subject to interruption. The availability of large quantities of natural gas will further allow the United States to consume a predominantly domestic supply of gas.

1.2. NATURAL GAS RESOURCES CLASSIFICATION

Unconventional natural gas resources have grown in importance as a complement to conventional fossil fuels as world energy demand has increased. Figure 1.2 shows the geologic nature of the most major sources of the natural gas in the United States. According to the EIA, natural gas reservoirs are categorized into conventional and unconventional natural gas resources.

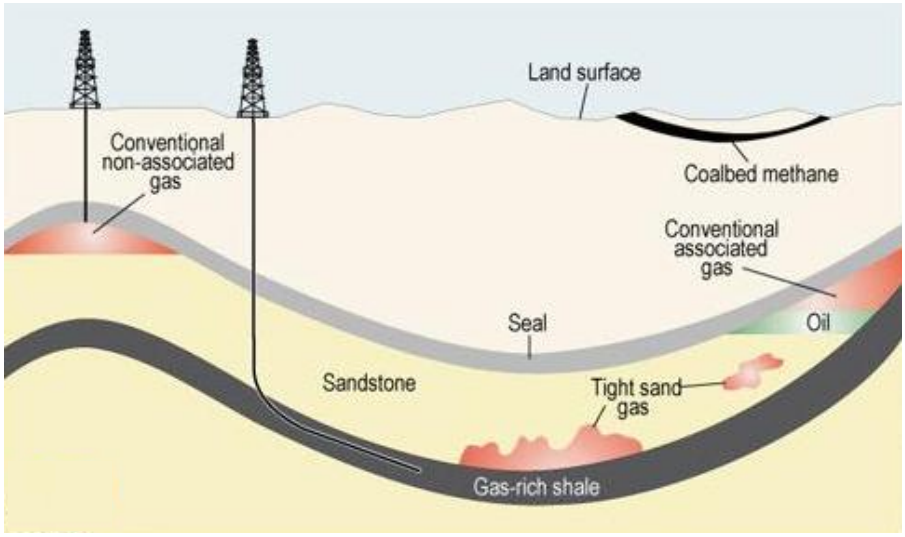

Figure 1.2. Geological Schematic of the Natural Gas Resources (Source: EIA)

1.2.1. Conventional Natural Gas Resources. Conventional natural gas occurs in porous sandstone and carbonate (limestone and dolomite) reservoirs. These reservoirs contain the gas in interconnected pore spaces that allow flow to the wellbore. The gas in the pores can move from one pore to another through smaller pore throats that create permeable flow through the reservoir. In conventional natural gas reservoirs, the gas is often sourced from organic-rich shales proximal to the more porous and permeable sandstone or carbonate. These resources are relatively shallower than unconventional natural gas reservoirs. The conventional gas accumulations can be found in two forms, associated natural gas and non-associated natural gas.

1.2.1.1 Associated natural gas. Associated gas accumulates in conjunction with oil. It encompasses the free gas formed as a cap onto the oil reservoir and the dissolved gas in oil under natural conditions. Natural gas associated with oil production was considered nuisance and used to be flared.

1.2.1.2 Non-associated natural gas. Non-associated natural gas resource has no or insignificant amount of crude oil in contact with the gas.

1.2.2. Unconventional Natural Gas Resources. Unconventional gas reservoirs occur in low permeability (tight) formations such as tight sands and carbonates, coal, and shale. In unconventional gas reservoirs, the gas is often sourced from the reservoir rock itself (tight gas sandstone and carbonates are an exception). Because of the low permeability of these formations, it is typically necessary to stimulate the reservoir to create additional permeability. Hydraulic fracturing of a reservoir is the preferred stimulation method for gas shales. Differences between the four basic types of unconventional reservoirs include:

1.2.2.1 Shale gas. Gas shales are fine grained, organic rich, sedimentary rocks. Shale formations act as both a source of gas and as its reservoir, unlike conventional gas reservoirs. It is called sometimes gas-rich shale. Natural gas is stored in shale in three forms: free gas in rock pores (micro-porosity), free gas in the local natural fractures (macro-porosity), and adsorbed gas onto organic matter (kerogen) and mineral surfaces (nano-porosity). These different storage mechanisms affect the speed and efficiency of gas production. The low permeability of the shale greatly inhibits the gas from migrating to more permeable reservoir rocks. Without horizontal drilling and hydraulic fracturing,

shale gas production would not be economically feasible because the natural gas would not flow from the formation at high enough rates to justify the cost of drilling and operations. Horizontal drilling and hydraulic fracturing have made shale gas an economically viable alternative to conventional gas resources.

1.2.2.2 Tight sand gas. Tight gas formations refer to sandstone and carbonate reservoirs with in situ effective permeabilities to gas equal to or less than 0.1 md. The natural gas is sourced outside a reservoir and migrates upward the reservoir over time (millions of years). Its migration ability is limited, due to reduced permeability in the sandstone. Tight sand gas accumulations occur in two different depositional settings, basin-centered gas and continuous gas accumulations as shown in Figure 1.2. Others are found in low permeability reservoirs in conventional structural, stratigraphic or combinations traps.

1.2.2.3 Coal-bed methane. Coal-bed methane does not migrate from shale, but it is generated during the transformation of organic material to coal. Wells produce from the coal seams which act as source and reservoir of the natural gas. Wells frequently produce water as well as natural gas. Hydraulic fracturing of coal-bed methane is strictly prohibited, because coal is found near surface water resources. This gas source of coal-bed methane natural gas are mostly shallow as the coal matrix does not have the strength to maintain porosity under the pressure of significant overburden thickness as illustrated in Figure 1.2.

1.2.2.4 Gas hydrate. Gas hydrates occur abundantly in nature, both in Arctic regions and in marine sediments. Gas hydrate is a crystalline solid consisting of gas molecules, usually methane, each surrounded by a cage of water molecules. It looks very much like water ice.

1.3. THE NATURAL GAS SOURCE PYRAMID

The concept of the resource pyramid was introduced by Masters et al. (1980). The concept is that all natural resources are distributed log-normally in nature. Aguilera et al. (2008) incorporated many parameters such as endowments, reservoir quality and delivery speed in the resource pyramid. Figure 1.3 shows endowment of conventional gas, tight gas, shale gas and coal-bed methane reservoirs. The diagram also illustrates the principle

of the resource triangle. Endowment is the summation of cumulative gas production, reserves and undiscovered gas. Delivery speed, which controls the definitions of flow units, decreases as we move down the pyramid from conventional to unconventional gas reservoirs.

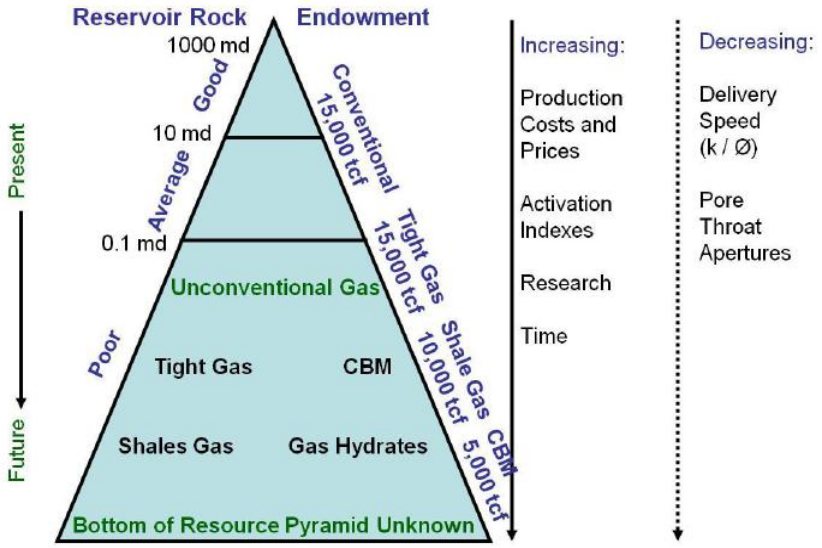

Figure 1.3. World Gas Resource Pyramid
(Adopted from Aguilera et al., 2008)

Figure 1.3 suggests that as you go deeper into the resource pyramid, the reservoirs are lower grade and the delivery speed become low, which usually means the reservoir permeability is decreasing and the rock pore structure becomes abstruse. These low permeability reservoirs, however, usually have much larger endowment than the higher quality reservoirs. As with other natural resources, low quality deposits of natural gas require improved technology and adequate gas prices before they can be developed and produced economically. However, the size of the deposits can be very large but difficult to develop, when compared to conventional or high-quality reservoirs.

1.4. CHALLENGES IN SHALE GAS SUBMICRON CHARACTERIZATION

The pore network, reservoir quality, and mechanisms of fluid flow in gas shales, are significantly different from those of conventional reservoirs and nonorganic fine-grain sediments. Not been well understood, they are complex and challenging. Advanced and qualified analysis tool such as submicron pore imaging and high pressure mercury porosimetry are required to quantify the petrophysical properties of shale gas.

Productive shale gas systems are composed of four classes of porous media: nonorganic, organic, natural fractures, and hydraulically induced fractures. The shale matrix is comprised of predominantly clay minerals, quartz, pyrite, and organic matter. The role of organic matter in gas-shale, which is poorly understood, can be important in terms of petrophysical properties, as well as migration and production. Organic-matter pores are only a few nanometers in diameter which could have a significant adsorbed gas content compared to the free gas content (Ambrose et al., 2010).

1.5. RESEARCH SCOPE

Gas storage and flow behavior in the shale gas rocks are complex and hard to identify by conventional core analysis. This study utilizes multifarious analysis techniques from material science, petrophysics, petrology and geochemistry to characterize North American shale gas samples from Utica, Haynesville, and Fayetteville shale gas plays. The scheme of this research is illustrated in Figure 1.4, which shows a successive series of the conducted experiments on the shale gas research which include mercury porosimetry, wettability measurements, submicron pore imaging, clay mineralogy, geochemistry analysis and gas flow modeling.

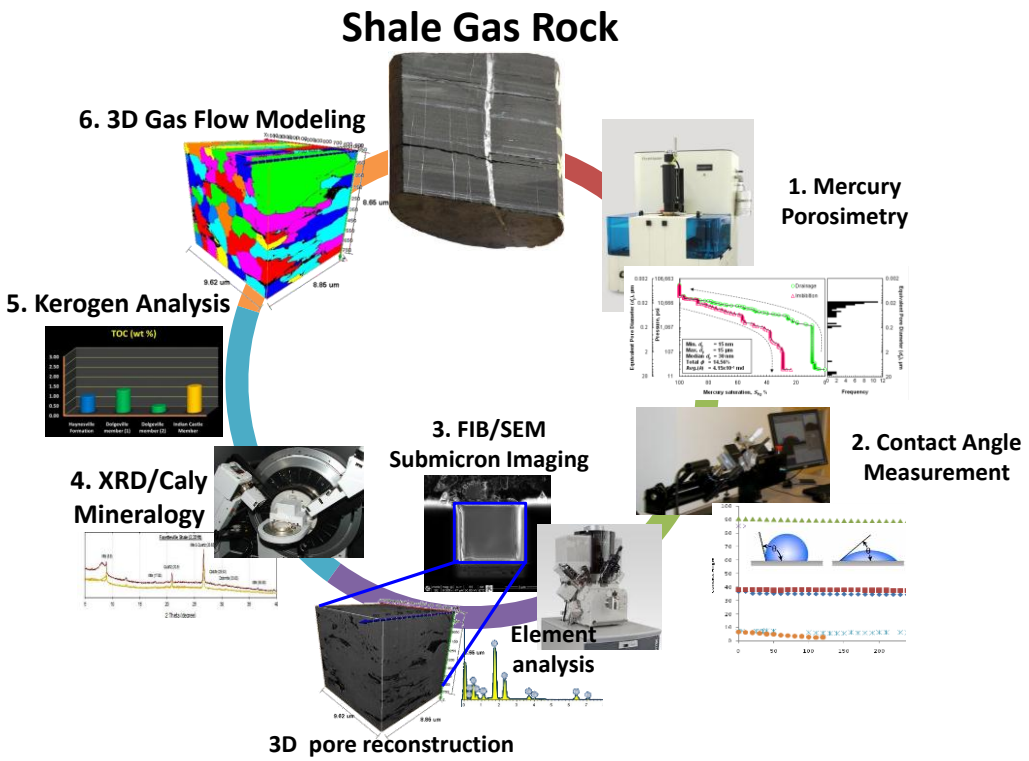

Figure 1.4. Shale Gas Research Workflow

High pressure (up to 60,000 psi) mercury porosimetry analysis (MICP) was used to measure the pore size distributions. Contact angle measurements were performed on the shale gas samples, and the effect of various fracturing fluid additives on their wettability was tested. In situ dual-beam microscope (Scanning Electron Microscope and Focused Ion Beam, also called SEM-FIB) was exploited to image and reconstruct the original pore structure of shale gas samples. The work used X-ray diffraction (XRD) to semi-quantify shale gas clay and non-clay minerals. Moreover, palynofacies analysis provided valuable information about kerogen type and its degree of thermal maturation, which are key parameters in shale-gas exploration. It qualitatively allowed the estimation of important organic geochemical parameters such as vitrinite reflectance (R_o %) and numerical thermal alteration index (TAI).

The aims of this study are to look into the submicron pore structure of shale gas and determine the potential effects of organic matter (kerogen), rock mineralogy on pore

types, pore networks and permeability. The impact of fracturing fluid additives on wettability alteration is investigated. The quantitative and qualitative geochemical analysis is carried out to obtain valuable information about kerogen type and its degree of thermal maturation. Furthermore, a robust, detailed tomography procedure using a dual-beam (SEM-FIB) instrument is successfully developed to characterize the submicron-pore structures. Table 1.2 presents the essential data of the examined shale gas samples in this study.

Table 1.2. Examined Shale Gas Samples Data
(Sources: 1. Baker-Hughes Company and 2. SouthWest Energy Company)

Sample No.	Shale Play	Formation	Sample Depth, ft	Well Location	Field Name /Province
1	Haynesville[1]	n/a	12,000	Rusk County	Texas
2	Utica[1]	Indian Castle	4,649	St. Lawrence Lowlands between Montreal and Quebec City	Quebec, Canada
3		Dolgeville	4,878		
4		Dolgeville	5,197		
5	Fayetteville[2]	n/a	2,351	10N, range 16W, section 36	Van Buren, Arkansas

1.6. THESIS OVERVIEW

This first section begins with introducing the importance of natural gas industry. It also describes the main challenges in acquiring the petrophysical characteristics of shale gas and why it is necessary to better understand the problem. It also outlines the objectives of this work.

Section 2 is a literature review of submicron pore analysis techniques and the palynofacies analysis. It is intended to serve as refresher of the roots of the micro-structural studies of gas shales.

Section 3 presents the results of the mercury porosimetry of Haynesville and Utica shale samples. A detailed tomography procedure using SEM-FIB machine is illustrated. It displays the porosimetry results of 3D submicron pore model. It also presents the X-ray diffraction and wettability results.

Section 4 presents the geochemical analysis results of the organic matter.

Section 5 summarizes the conclusions and recommendations of this work.

2. LITERATURE REVIEW

2.1. SHALE GAS INDUSTRY IN THE UNITED STATES

Shale gas resources are more abundant and less expensive than other domestic natural gas supply alternatives that could replace them, and they are expected to play a significant role in future domestic natural gas markets (EIA). Consequently, their future absence or presence is expected to have a significant impact on the average cost of natural gas production and prices, which in turn would affect natural gas imports and consumption.

Shale gas is the second largest unconventional energy resource after heavy oil. Shales have high abundance of organic matter (kerogen) that sets shales among the best candidate source rocks for petroleum and natural gas generation. However, shale gas reservoirs present a unique problem to the petroleum industry. They contain natural gas in both the pore spaces of the organic matter as free gas and on the surface of the rock grains as adsorbed gas (Wang and Reed, 2009). Two major enhancement techniques are used to extract natural gas from shale. Horizontal drilling is used to provide greater access to the gas trapped deep in the producing formation. Hydraulic fracturing (commonly called “fracking” or “hydrofracking”) to unlock the hydrocarbons trapped in shale formations by opening cracks (fractures) in the rock and allowing natural gas to flow from the shale into the well. This is a complicated problem in understanding the shale gas storativity.

Historically, the first commercially successful gas production in the US came from what would now be considered an unconventional reservoir in the Appalachian Basin in 1821. Currently, some of the largest gas fields in North America are unconventional, shale gas plays such as the Barnett Shale of the Fort Worth Basin, the Marcellus Shale and Utica Shale of the Appalachian Basin, and the Haynesville Shale of the North Louisiana Salt Basin. Figure 2.1 presents the major shale gas plays in the US.

Figure 2.1. United States Shale Gas Plays Map
(Source: US Energy Information Administration, 2010)

Over the past decade, the combination of horizontal drilling and hydraulic fracturing has allowed access to large volumes of shale gas that were previously uneconomical to produce. The production of natural gas from shale formations has rejuvenated the natural gas industry in the United States. Three major shale gas plays are concerned in this study, which include Utica Shale, Haynesville Shale and Fayetteville Shale gas plays.

2.1.1. The Utica Shale. The Utica Shale play lies between 3,000 and 7,000 thousand feet beneath the Marcellus Shale but extends further northwest and much further southwest of the Appalachian Basin region as shown in Figure 2.2. Utica Shale consists of three members, Indian Castle at the top, Dolgeville in the middle and Flat Creek at the bottom of the play. Utica Shale rocks are Ordovician in age, but Marcellus is Devonian shale.

According to the data provided by the US Energy Information Administration (EIA) and the United States Geological Survey (USGS), the Utica Shale is thicker than the Marcellus and it is more geographically extensive (about twice as extensive as the

Marcellus). Thickness and widespread geographical extent indicate it may become an enormous natural gas resource.

At this point, while limited production has occurred in the Utica Shale, it is hard to estimate its size. This might be attributed to the fact that Utica Shale has not been thoroughly evaluated and little public information is available about its organic content, the thickness of organic-rich intervals and how it will respond to horizontal drilling and hydraulic fracturing. Therefore, this research aims to tackle the submicron pore evaluation of Utica Shale.

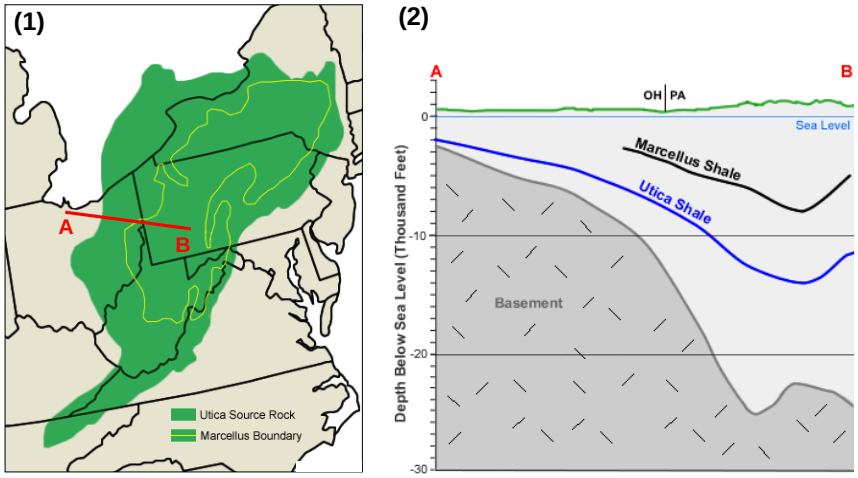

Figure 2.2. Utica Shale Gas Play Geographic and Cross Section Map (Source: The US Energy Information Administration, EIA and the United States Geological Survey, USGS)

2.1.2. The Haynesville Shale. The Haynesville Shale is situated in the North Louisiana Salt Basin in northern Louisiana and eastern Texas with depths ranging from 10,500 to 13,500 ft as reported by Halliburton Energy Services. The Haynesville is an Upper Jurassic-age shale bounded by sandstone (Cotton Valley Group) above and limestone (Smackover Formation) below (Johnson et al., 2000), as shown in Figure 2.3.

Period		Group/Unit
Cretaceous		Navarro
		Taylor
		Austin
		Eagle Ford
		Tuscaloosa
		Washita
		Fredericksburg
		Trinity Group
		Nuevo Leon
Jurassic	Upper	Cotton Valley Group
		Haynesville
		Smackover
		Norphlet
	Middle	Louann
	Lower	Werner
Triassic	Upper	Eagle Mills

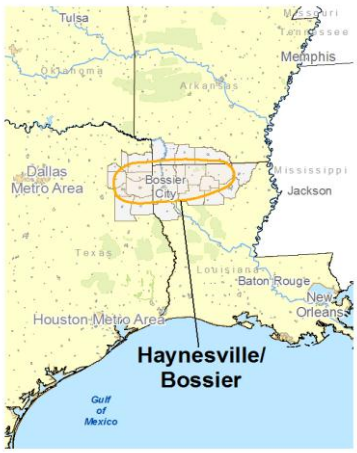

Figure 2.3. Stratigraphy and Location Map of the Haynesville Shale (Source: Schlumberger, 2005)

In 2007, after several years of drilling and testing, the Haynesville Shale made headlines as a potentially significant gas reserve, although the full extent of the play will only be known after several more years of development are completed. The daily gas production date reported by EIA in the beginning of March 2011 shows Haynesville Shale is currently producing about 5.5 Bcf which surpasses the Barnett production by 0.25 Bcf as presented in Figure 2.4. This growth is mainly attributed to increasing drilling activities, improving the drilling experience and expanding the regional infrastructure of Haynesville Shale.

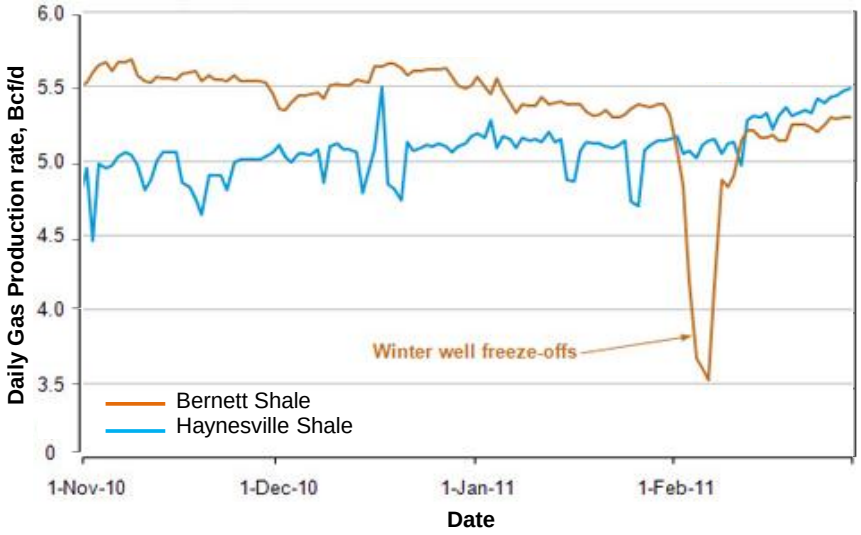

Figure 2.4. Haynesville and Barnett Shale Daily Gas Production (Source: EIA, 2011)

The Haynesville Shale covers an area of approximately 9,000 square miles with an average thickness of 200 to 300 ft, estimated by Boughal and Berman in 2008 respectively. The thickness and areal extent of the Haynesville has allowed operators to evaluate a wider variety of spacing intervals ranging from 40 to 560 acres per well (Sumi, 2008). The Haynesville formation has the potential to become a significant shale gas resource for the U.S. with original gas-in-place estimates of 717 Tcf and technically recoverable resources estimated at 251 Tcf (Navigant Consulting Co., 2008).

2.1.3. The Fayetteville Shale. The Fayetteville Shale is situated in the Arkoma Basin of northern Arkansas and eastern Oklahoma over a depth range of 1,000 ft to 7,000 ft as illustrated in Figure 2.5. The Fayetteville Shale is a Mississippian-age shale bounded by limestone (Pitkin Limestone) above and sandstone (Batesville Sandstone) below (Hillwood, 2007).

Development of the Fayetteville began in the early 2000s. Between 2004 and 2007 the number of gas wells drilled annually in the Fayetteville shale jumped from 13 to more than 600, and the annual gas production for the shale increased from just over 100 MMcf to approximately 88.85 Bcf (Boughal, 2008).

The area of the Fayetteville Shale play is nearly double that of the Barnett Shale at 9,000 square miles, with well spacing ranging from 80 to 160 acres per well, and pay zone thickness averaging between 20 ft and 200 ft (Hayden et al., 2005).

Figure 2.5. Stratigraphy and Location Map of the Fayetteville Shale (Source: Schlumberger, 2005)

2.2. CLAY MINERALOGY AND STRUCTURE

The mineralogy of the rock surface has an influence on the overall wettability of the fluid-rock system. Clays are the dominant minerals in shales with illite, kaolinite, smectite, chlorite being the most common clays. Clays, compositionally, are a class of aluminum silicates and structurally they are complex with a wide range of properties. Clays have two basic building blocks which can be used to construct most of the clay minerals. The first is a tetrahedral silicate sheets with oxygen ions at the corners. The second is an octahedral arrangement where hydroxyl ions occupy the corners and surround magnesium to form brucite layer or aluminum ions to form gibbsite layer (Grim, 1968), as shown in Figure 2.6. Most of the clays are composed of sandwiches of these building blocks repeated over and over.

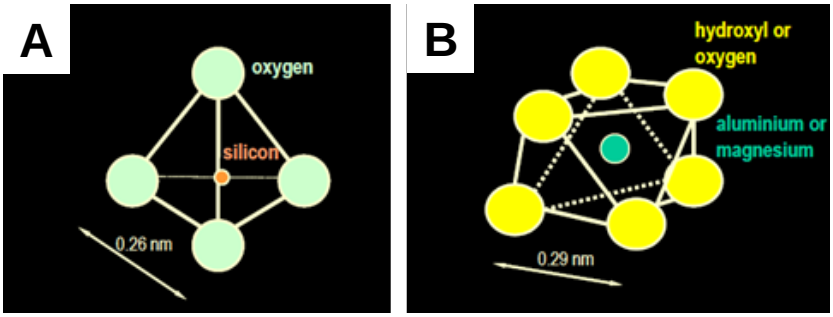

Figure 2.6. Basic Clay Two Building Blocks
(A) Silicate Tetrahedron and (B) Aluminum or Magnesium Octahedron

Most of the clays exhibit 2:1 or three sheet sandwich structures, in which an aluminum-hydroxyl octahedral sheet is sandwiched between two oxygen-silicon tetrahedral sheets as presented in Figure 2.7. Illite is the most abundant clay mineral. These are nonexpanding 2:1 type layer clays. The prototype minerals for illites are muscovite and phlogopite. Illites do not exhibit interlayer swelling in water or organic compounds. Most of the substitution in illites occurs in the tetrahedral sheets. The compensating cation in illites is usually potassium. However, the illite layers do not separate from each other on contact with water and the potassium ions between the layers are not available for exchange. Only the potassium ions on the external surfaces are available (Sharma, 2006). The basal spacing d(001) of illite is 10 Å. A more detailed discussion of the structure of illite and its variable composition can be found in Moore and Reynolds (1989).

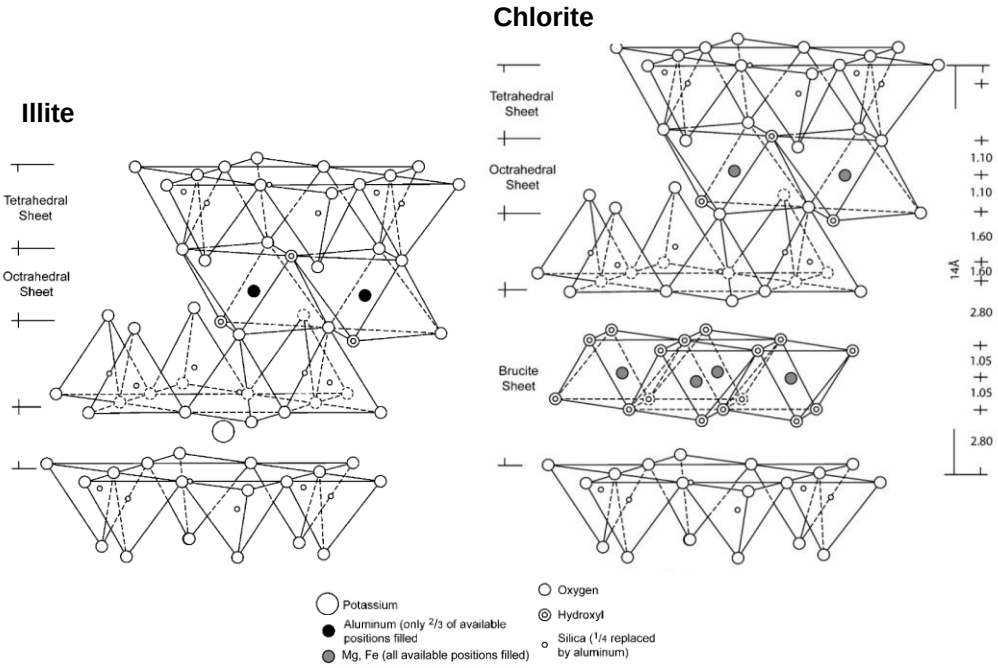

Figure 2.7. Diagrammatic Sketch of the Structure of Illite and Chlorite (Adopted from Murray, 2007)

Chlorite is commonly present in shales and also in underclays associated with coal seams. Clay mineral chlorites differ from well-crystallized chlorites in that there is random stacking of the layers and also some hydration. Chlorite is a 2:1 layer mineral with an interlayer brucite sheet $Mg(OH)_2$ as shown in Figure 2.7. There is quite a range of cation substitutions in chlorites, most commonly Mg^{2+}, Fe^{2+}, Al^{3+}, and Fe^{3+} (Murray, 2007).

Rock mineralogy and texture can be a critical component in the resource potential of shales (Sliwinski et al., 2010). Rocks with high silica (quartz) and low clay content typically have high Young's modulus and low Poisson's ratio making them more brittle and more prone to natural fractures and good candidates for fracture stimulation.

Clay minerals are very fine grained that X-ray methods, rather than hand specimen or optical methods, are used to identify. The X-ray techniques are considerably more involved than those for other types of minerals and differ in complexity depending on the detail required for identification.

2.3. SUBMICRON PORE ANALYSIS

The key to successful characterization of fluid flow behavior in shale gas plays is an understanding of the petrophysics of shale rocks and their submicron pore structures. A few studies have attempted to construct submicron pore structures.

2.3.1. Micro-Structural Studies. In 2007, Tomutsa et al. conducted an initial and intensive submicron pore imaging study using in situ dual beam device (Scanning Electron Microscope and Focused Ion Beam, also called SEM-FIB) to evaluate the petrophysical properties of chalk rocks. A successive milling process using the FIB was performed for 3D reconstruction. Maximum-inscribed-spheres (MIS) image processing method was exploited to compute the petrophysical properties by direct morphological analysis of the pore spaces.

However, several shale samples from Barnett and Haynesville shales and the Canadian Buckinghorse and Shaftesbury shales were examined by Chalmers et al. (2009) on dual beam device (SEM-FIB). The pore size distribution and mineralogy of these samples were identified to evaluate the importance of the meso- and microporosity in controlling the methane capacity.

Moreover, the pore network systems of the siliceous mudstones from Mississippian Barnett Shale were identified by Loucks et al. (2009) using scanning electron microscopy for imaging and Ar-ion-beam for milling process.

The potential effects of organic matter on the petrophysical properties. pore networks and fluid flow in gas shale systems were investigated by Wang and Reed (2009) based on gathered data from previous studies on Barnett Shale, such as SEM pore images data, gas adsorption test and geochemical analysis data.

Furthermore, serial investigations on types of porous constituents inherent to shale gas rocks were performed by Ambrose et al. (2010) utilizing the 2-D and 3-D reconstructed submicron pore models form SEM-FIB tomography. They developed a new gas-in-place equation which takes into account the sorbed methane.

Another study focused on SEM imaging for certain gas shales such as Barnett Shale, Fayetteville Shale, Floyd Shale and Frio Shale was performed by Sondergeld et al. (2010). A sequential ion beam milling (SEM-FIB) to acquire 256 slices of 10 nm thick for three-dimensional reconstruction was implemented. Moreover, they used other tools

for the petrophysical measurements, high pressure mercury capillary pressure (MICP) and Nuclear Magnetic Resonance (NMR).

A comprehensive comparative study of a variety of major gas shales which are Barnett, Eagle Ford, Fayetteville, Floyd, Haynesville, Horn River, Kimmeridge, Marcellus, and Woodford was conducted by study Curtis et al. (2010). Nevertheless, none of these studied shale samples were from Utica Shale. Dual beam (SEM-FIB) performed 300-600 steps of serial slicing with 10 nm slice thick. The extracted pore sizes from 3D reconstructed pore model were compared to the results of MICP and NMR analysis.

2.3.2. Organic Matter Pore Size. The pores in the mudrocks are dominantly nanometer in scale as small as 5 nm and they predominately exist in the organic matter as intraparticle pores (Loucks et al., 2009). Chalmers et al. (2009) found a significant portion of the total porosity is in organic-rich shales within the size ranges of 2 to 50 nm. Wang and Reed (2009) extensively estimated the kerogen nanopore sizes from 5 to 1,000 nm as shown in Figure 2.8. Ambrose et al. (2010) observed that organic matter have pores and capillaries with sizes less than 100 nm. Sondergeld et al. (2010) reported small pore sizes in kerogen, i.e. < 20 nm. Curtis et al. (2010) universally observed pores within the shale samples range from a few to hundreds of nanometers in diameter.

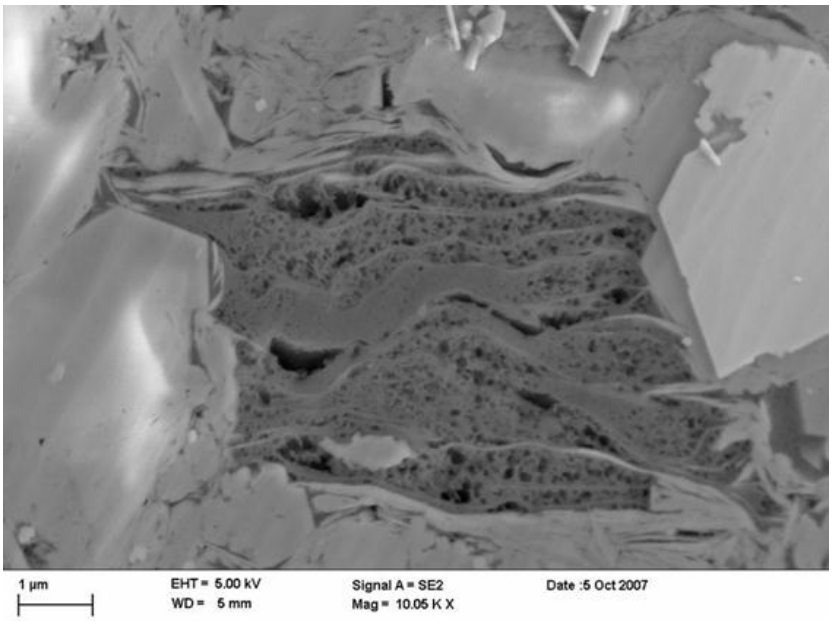

Figure 2.8. SEM Image of the Organic Matter
(Source: Wang and Reed, 2009)

2.3.3. Shale Gas Porosity Types and Magnitude. Five constituents of porosity types on the microscale were found in numerous shale gas samples by Sondergeld et al. (2010). They are located in organics, between grains, in pyrite framboids, fossils, within minerals and in the form of microcracks. Loucks et al. (2009) showed less abundance of nanopores are locally located in fine grained matrix areas as nano- to micro-intercrystalline pores in pyrite framboids. However, the majority of pores in some shales are located in the organic matter. Furthermore, Wang and Reed (2009) and Ambrose et al. (2010) highlighted that the inter-connected nano-pores of the organic material store a significant amount of free gas. Chalmers et al. (2009) showed that nano-porosity of gas shales increases the total porosity and surface area for methane sorption. Loucks et al. (2009) estimated that porosity in organic matter ranges from 0 to 25%. Wang and Reed (2009) concluded that the organic matter porosity is higher than porosity in nonorganic matrix by five orders of magnitude. Curtis et al. (2010) stated that kerogen in some shales has been found to have porosities of up to 50%.

2.4. PALYNOFACIES ANALYSIS

Palynofacies analysis as defined by Tyson (1995) is: “the palynological study of depositional environments and hydrocarbon source rock potential based upon the total assemblage of particulate organic matter.” Palynofacies is a term commonly used to describe the quantitative and qualitative palynological study of the total particulate organic matter assemblage contained in a body of sediment thought to reflect a specific set of environmental conditions, or to be associated with a characteristic range of hydrocarbon-generating potential (Tyson, 1993 and 1995). This term was first introduced by Combaz (1964) to describe the total microscopic image of the organic components. Then it became popular however, the definition varied between different authors. Some authors named the organic components “organic matter”, others “palynodebris” but still others “kerogen” (Carvalho, 2001). The term kerogen is today the most commonly used term to describe the organic components contained in sedimentary rocks (Tyson, 1993). Tyson (1993) used the term kerogen in a purely palynological sense to describe the dispersed particulate organic matter of sedimentary rocks that is insoluble in hydrochloric (HCl) and hydrofluoric (HF) acids.

Palynofacies analysis involves the identification of individual palynomorphs, plant debris and amorphous components, their absolute and relative proportions, size spectra and preservation states. It is an interdisciplinary technique that forms the natural interface between palynology, sedimentology and organic geochemistry (Tyson, 1993).

In this study, kerogen assemblages are categorized into four main groups similar to those identified by Ibrahim et al. (1997) namely, structured phytoclasts, degraded phytoclasts, opaques, and palynomorphs

2.5. KEROGEN TYPE

Shale plays with abundance of the organic material are more attractive to the gas market than other regular shales. The organic matter in shale is named kerogen. Kerogen is a product of anaerobic decomposition of organic matter from dead plants and animals. It is the dispersed sedimentary organic matter that is resistant to the mineral acids hydrochloric acid (HCl) and hydrofluoric acid (HF) (Tyson, 1993).

At deeper burial depths, high temperature and high pressure transform the kerogen through liquid bitumen into liquid petroleum product (Tiab and Donaldson, 1996). If oil produced this way stays trapped in a source rock, the overburden and the high temperature at deeper depths results in cracking of oil into gas.

The classification of kerogen type by Tyson (1993) for routine source rock evaluation was followed in the present study.

2.5.1. Kerogen Type I. It is deposited in a relatively quiet lacustrine environment (deposition in lakes) (Tissot, 1984). It encompasses alginitic material derived from chlorococcale algae, prasinophyte algae, cyanobacteria and some thiobacteria. It is highly oil prone with as much as 70% wt. of the organic matter transforming into oil depends on the level of thermal maturation.

2.5.2. Kerogen Type II. It is known to originate from herbaceous plants. It includes amorphous organic matter, but sporopollenin palynomorphs, cuticle and non-cellular membraneous debris are also included. This type of kerogen produces both oil and gas.

2.5.3. Kerogen Type III. It is orange or brown, translucent, phytoclasts or structureless materials. It is originated from woody matter deposited in marine or non-marine environment and have undergone a moderate degradation. It is classified as gas prone material. It can generate dry gas as less than 30% wt. of the organic matter that can be transformed into oil.

2.5.4. Kerogen Type IV. It is opaque to semi-opaque, black, or very dark brown particles, representing oxidized or carbonized phytoclasts. It is considered as inert material.

2.6. ORGANIC MATTER THERMAL MATURATION

Thermal maturation is the chemical change induced by post-depositional heating over time that transforms sedimentary organic matter into hydrocarbon (Peters and Cassa, 1994; Traverse, 2007). Source rocks are thermally classified into immature, mature, and post-mature depending on the temperature level they were subjected to (Peters and Cassa, 1994). Color changes in the exine of fossil palynomorphs (e.g. spores and pollen) have

long been used to interpret the degree of thermal maturation of potential source rocks. Figure 2.9 presents the color chart of the spore/pollen by Traverse (2007).

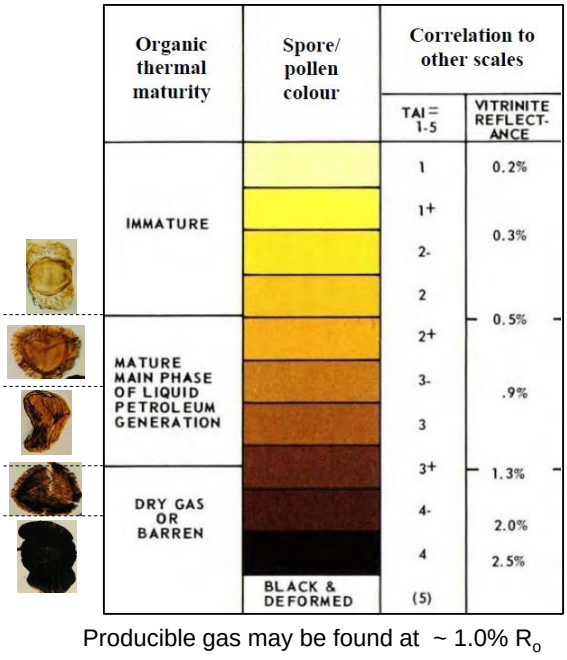

Figure 2.9. Chart of the Spore/Pollen Colors
A Comparison of the Organic Thermal Maturity, Thermal Alteration Index (TAI), Vitrinite Reflectance (R_o%) and the Color of the Spore/Pollen (Traverse, 2007)

As the organic matter matures, it breaks down to generate oil and gas, the rate of oil and gas generation is slow at first, then increases rapidly, then diminishes again as illustrated in Figure 2.10. Initially, oil is the main product, but at higher maturities oil generation declines and gas generation increases (Oehler, 1983).

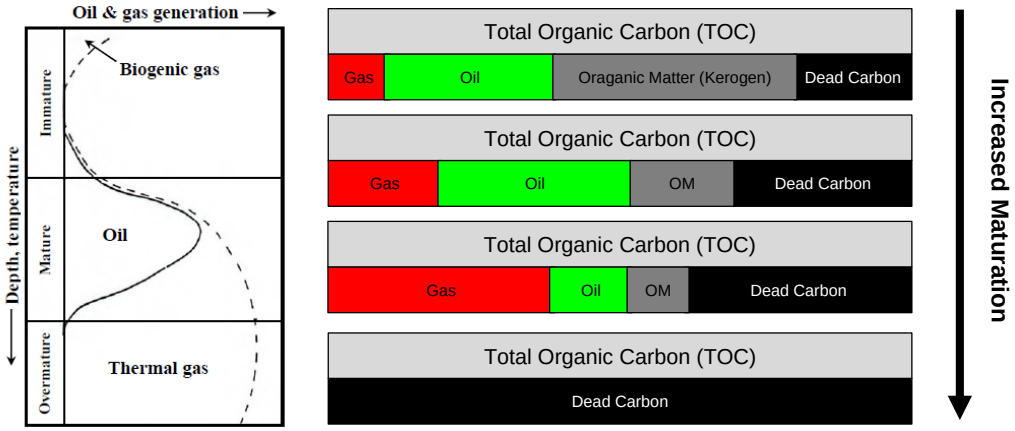

Figure 2.10. Oil and Gas Generation
A Function of Increasing Sediment Burial and Thermal Maturation (Oehler, 1983 and Modified after Jarvie, 2004)

The maturity range over which most of the oil is generated is called the "oil window" and the rocks generating that oil are said to be "mature". Rocks that have not yet reached that stage are called "immature" and rocks that have passed through that stage into the gas generating phase are called "over-mature or post-mature" (Oehler, 1983). Shale gas rocks are usually have post mature organic matters which are capable to produce dry gas.

2.7. TOTAL ORGANIC CARBON

Total organic carbon (TOC) is not a direct measure of hydrocarbon source potential. Instead, a combination of several proxies in addition to TOC must be considered (e.g. lithologic composition, sedimentation rate, kerogen type, thermal maturation, basin redox conditions, etc.). TOC values are measured in terms of weight percentage of organic carbon. 1% wt. of TOC represents 1 gram of organic carbon in 100 gram of sediment sample (Jarvie, 1991). Candidate source rocks under appropriate conditions should have TOC greater than the accepted minimum limit 0.4 wt. %.

The TOC for a given source rock is composed of three fractions, namely organic carbon in the extractable hydrocarbons, organic or live carbon that can be transformed into hydrocarbons, and dead carbon that cannot yield hydrocarbons (Jarvie et al., 2007) as

shown in Figure 2.11. This clearly implies that TOC content will diminish in a source rock with hydrocarbon expulsion.

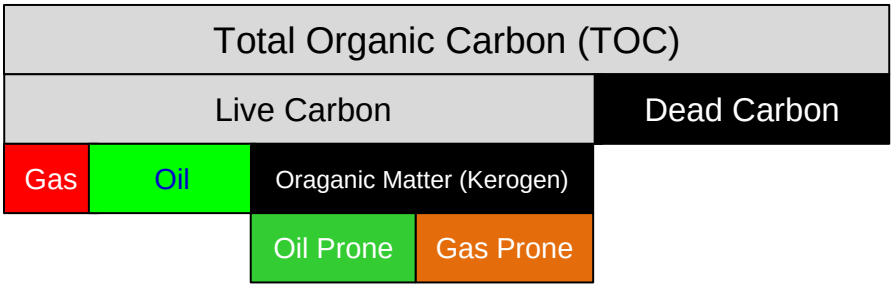

Figure 2.11. Distribution of the Organic Matter in the Rock Sample

2.8. ESTIMATED KEY GEOCHEMICAL PARAMETERS

Several studies have demonstrated the strong correlation between data obtained from palynofacies analysis and those from instrumental geochemical analyses (e.g. Zobaa et al., 2007, 2009; El Beialy et al., 2010). Detailed list of the pros and cons of both methods in organic maturation studies can be found in Brooks (1981). However, the relatively inexpensive nature of palynofacies analysis makes it powerful in preliminary exploratory studies limited by tight budgets. The estimated geochemical parameters are numerical thermal alteration index (TAI) and vitrinite reflectance (R_o %).

3. SUBMICRON PORE CHARACTERIZATION

Gas storage and flow behavior in the shale gas rocks are complex and hard to identify by conventional core analysis. Qualitative and quantitative characteristics of shale-gas source rock are used by petrophysicists, geochemists and reservoir engineers. These include submicron pore structure analyses, which is important in the derivation of rock capillarity, wettability and storativity. Shale gas rocks hold large quantities of hydrocarbon reserves that have made significant impact on North American oil and gas market since early 2000s. The ambiguity behind gas storativity and deliverability can be demystified through the understanding of the relationship between organic matter content and porosity. This section presents clustering analysis techniques from material science, petrophysics, and petrology to characterize North American shale gas samples from Utica, Haynesville, and Fayetteville shale gas plays.

3.1. MERCURY POROSIMETRY

Mercury (Hg) is a toxic material that has been used in rock laboratories as an indirect measure of rock capillarity and porosimetry. These experiments are considered destructive, expensive, and time consuming. Nevertheless, mercury porosimetry has been widely accepted as a mean to characterize porous solids with respect to their pore volume (porosity) and pore size distribution over a wide range of pore sizes. Mercury is nonwetting phase and it can only access interconnected pores. The volume of mercury that can enter pore spaces is limited by the maximum pressure attained during analysis.

3.1.1. MICP Methodology. Mercury porosimetry analysis of shale gas rocks is essential and difficult to be achieved by the ordinary porosimeters. The petrophysical properties of shale gas rocks are significantly different from those of conventional oil and gas reservoirs because of the nano-scale pores and unique pore structure of shale gas rocks. Moreover, shale gas rocks are practically classified as impenetrable material (i.e. they have ultra-low permeability). Therefore, high mercury intrusion pressure (up to 60,000 psi) instrument as shown in Figure 3.1 offers a great tool to measure shale gas pores at nano-scale.

Figure 3.1. Mercury Porosimetery Instrument
POREMASTER® (Source: Quantachrome Instruments Company)

When an incremental pressure is applied, mercury begins intruding into open connected pores. Effective porosity can only be quantified using this method. Once pressure reaches the upper limit, the extrusion process begins, while pressure decreases incrementally to atmospheric pressure (~14.7 psi). Both pressure and cumulative intruded and extruded mercury volumes are being monitored.

The mercury capillary pressure curves are dependent upon, pore size distribution and tightness, rock and fluid type and saturation history (intrusion and extrusion processes). Data extracted from saturation and desaturation curves always show differences in pore size distribution. Extrusion data often indicate smaller pores than intrusion data. This discrepancy is attributable to intrusion and extrusion hysteresis, which is dependent on the saturation process (Leverett, 1941). It is also likely due to alterations in the advancing and receding mercury contact angles, and to mercury entrapment. Mercury porosimetry is traditionally calculated as:

$$p = \frac{-2\sigma\ cos\theta}{r} \quad (1)$$

where, p is the pressure that must be applied to nonwetting liquid (mercury) to penetrate cylindrical pores of radius r, and σ and θ are the mercury surface tension and contact angle, respectively. This equation indicates that, as pressure increases, the mercury intrudes into progressively narrower pores as long as the surface tension and contact angles remain constant.

3.1.2. MICP Results and Discussion. Twelve samples were analyzed for analyses of capillary pressure using high-pressure mercury injection. Core Lab used a PoreMaster 60 mercury injection instrument for testing as shown in Figure 3.1. Samples were subjected to an injection pressure of up to 60,000 psia.

High pressure mercury capillary pressure (MICP) has produced representative and reproducible results for conventional reservoir rocks. However, for shale gas rocks, the scenario is almost impossible to reproduce due to the shale tightness. Only two of 12 attempts have been successful, although high injection pressures up to 60,000 psi were applied. This pressure level is still greater by a factor of 5 than that determined by curve of water drainage displaced by air.

This work used small volumes and weights (1−3 grams), despite claims by some researchers that this approach can minimize the credibility of capillary pressure values. However, studies by Wardlaw and Taylor (1976), Ghosh et al. (1987), and Kopaska-Merkel and Amthor (1988) have shown that small sample weight has no significant effect on mercury porosimetry.

This project carried out two successful MICP experiments using Utica and Haynesville shale samples. Figure 3.2 presents mercury intrusion and extrusion curves of Utica shale alongside the resulting pore size histogram. It shows possible tiny fractures that exhibit little instant intrusion due to the raise of mercury head in the penetrometer. The crooked curve of the intrusion and extrusion process is an indicator of various pore sizes and/or different flow units. Pore throat diameter can be calculated using equation 1 and a known mercury surface tension of 480 dynes/cm and contact angle of 140° for mercury. Figure 3.2 shows also a statistical pore size distribution based on intruded mercury volume data. The resulting Utica shale median pore throat diameter was 30 nm. Most of the intruded mercury occurred between 3,500 and 21,000 psi, a level corresponding to a pore throat diameter of 10−60 nm and certainly a result of shale pore

structure and mineral texture. Residual mercury saturation was 23.3%. Sondergeld et al. (2010) reported that MICP porosimetry underestimates the pore radii more than Scanning Electron Microscope (SEM) imaging results. Because this method is destructive and sponsors can provide only limited quantities of shale gas rock, this work did not include the comparison study originally proposed. However, future studies should demonstrate the correlation between MICP and three-dimensional SEM pore histogram results.

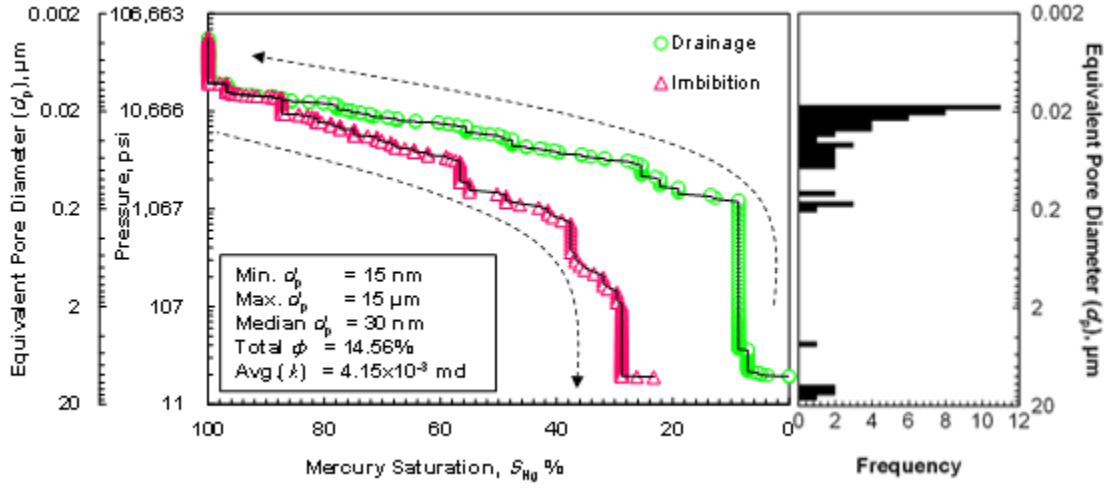

Figure 3.2. MICP Test Results of Utica Shale
Mercury Intrusion and Extrusion Data and Pore Size Distribution of Intrusion Data for Utica Shale, Dolgeville Fm., at a Depth of 5,197 ft

Numerous attempts have been made to relate the permeability of a solid to intrinsic and more readily measurable properties, such as porosity and pore diameter. Kozeny models the flow of fluids across straight cylindrical channels in a bed of rock by combining Darcy's and Poiseuille's laws to obtain

$$k = \frac{\phi\, d_p^2}{32\,\tau} \tag{2}$$

where ϕ is the rock porosity, d_p is the average (mean volume) diameter of the pores, and τ is the tortuosity coefficient. The MICP analysis assumes the tortuosity coefficient is equal to 1 (i.e., the pores are assumed to be straight, cylindrical capillaries). Using the Kozeny simplified formula, the permeability of Utica shale sample was estimated to 4.15×10^{-3} md, with a porosity of 14.56%.

Figure 3.3 presents another successful MICP test for the Haynesville shale sample. It suggests that about 35% of the mercury was initially intruded before any pressure was applied. It also shows a possible fracture 15 µm wide. This crack could tremendously increase gas deliverability and storability. The computed permeability represents the majority of nanopore networks. Most mercury intrusion occurred between 10,600 and 60,000 psi, which is equivalent to a pore throat diameter of 4−20 nm. The Haynesville shale has extremely low permeability of 1.38×10^{-4} md, mainly because of the nanopore level, which is peculiar to shale gas. The total entrapped mercury is 61.3%, which includes the remaining mercury in the possible open crack. Thus, the net residual mercury in the nanopores would be 26.66%.

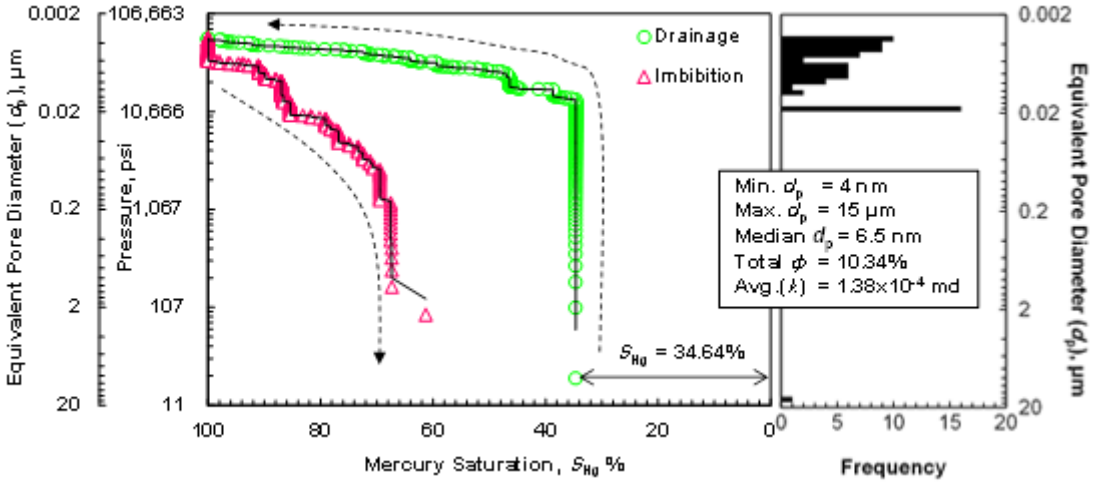

Figure 3.3. MICP Test Results of Haynesville Shale
Mercury Intrusion and Extrusion Data and Pore Size Distribution of Intrusion Data for Haynesville Shale at a Depth of 12,000 ft

3.2. SUBMICRON-SCALE PORE IMAGING

3.2.1. Dual-Beam Microscope. The dual-beam system (Scanning Electron Microscope and Focused Ion Beam, also called SEM-FIB) has been widely used in material science studies. It is especially useful for three-dimensional microscopy and material characterization. It is currently considered the best method for sectioning and imaging the microstructure of gas shale samples. Its electron gun offers in situ imaging, and the focused ion beam provides simultaneous sequential milling. FIB milling gun uses Ga^+ ions accelerated at high voltage to bombard the shale surface and sputter away material via momentum transfer. Many electron detectors are associated with a dual-beam microscope. This work relied primarily on three detectors to detect the electrons and rays ejected from the targeted specimen when it was attacked by the electron beam. The ejected electrons included secondary electrons (SE) and backscattered electrons (BSE) for imaging. An energy dispersive spectroscope (EDS) detector permitted element mapping. A BSE detector is preferable for imaging because it minimizes surface electron charges. However, an SE detector can also produce satisfactory images.

Figure 3.4 shows the standard dual beam setup for shale gas serial sectioning and imaging. The stage must be tilted at 52° to make the ion beam normal to the specimen.

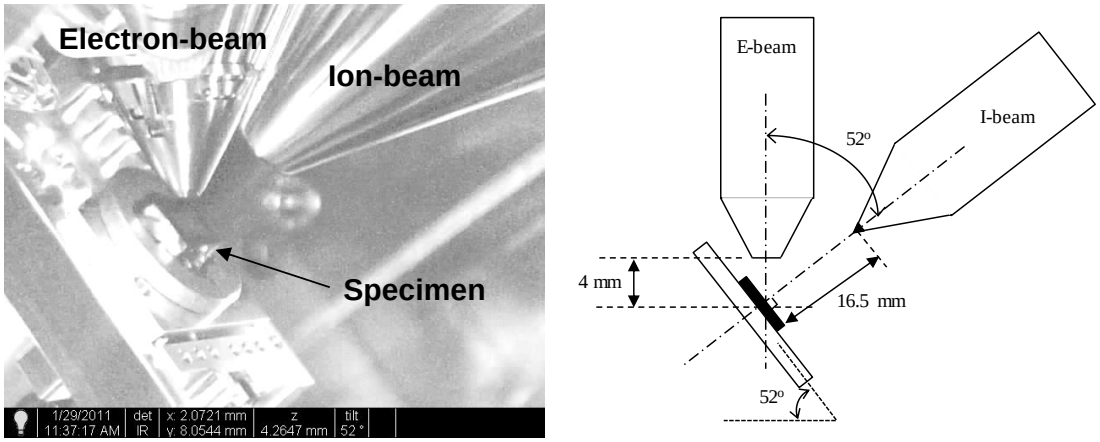

Figure 3.4. Dual Beam Microscope with Loaded Shale Sample at 52° Tilt

Shale gas rock, however, is nonconductive. Super electron charges are very likely to occur on the exposed surface. Therefore, this case demanded the use of a low voltage electron beam (2−5 kV) on the SEM side when a high electron beam current (0.17−1.4 nA) was used. This technique provides better image at high magnification.

3.2.2. SEM-FIB Tomography Procedure. Following is a detailed description of the optimum submicron pore imaging procedure used in this study.

3.2.2.1 Saw and polish small rock slices. Specimens were prepared by sawing the rock into pieces measuring 5×5×2 mm. Figure 3.5 shows two common types of fractures, nonconductive and conductive, that have been observed in Utica shale while sawing; they are marked by A and B respectively. Conductive fractures may be drilling induced or natural, whereas nonconductive fractures are mostly healed by calcite. Macro conductive fractures are bridge-like, and they act along micro- or nano fractures to transport the adsorbed and free gas to the wellbore.

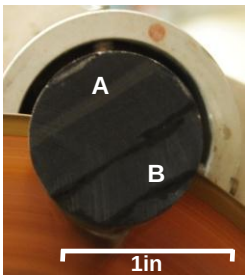

Figure 3.5. Sawing a Utica Shale Sample
Indian Castle Fm. Sample at a depth of 4,649 ft: (A) Calcareous healed natural fractures, and (B) Either conductive natural fractures or drilling-induced cracks

Specimens should be polished with the finest sand paper to give them a flat, smooth surface for better milling rate and time. Polishing was once believed to destroy the natural surface features; however, FIB mills beneath the surface to explore the undamaged clay structure. Fresh surfaces were usually used, although these require a longer milling time due to nonuniform milling surface.

3.2.2.2 Glue and coat sample plates. The specimen was attached to an aluminum stub using carbon glue. Image drift is the most challenging problem in three-dimensional image stacking. Three types of drifts are possible: specimen drift, mechanical stage drift, and ion beam drift. Carbon glue can effectively attach the specimen to the stub, dramatically reducing specimen drift. To avoid mechanical stage drift during the FIB slicing procedure, the sample dimensions were kept as small as possible. Nonetheless, slight drift can occur as a result of an ion beam alignment disorder. A calibrated FIB with a highly focused ion beam alignment was used to eliminate this drift. Since shale rock is nonconductive material, a coating of gold and palladium is the most suitable material to increase sample conductivity and to lessen the electron charge on the surface. Moreover, this coating prevented interference with the carbon that exists naturally in the specimen within the organic matter. Figure 3.6 presents the pinned specimen in the stub holder. The latter will be mounted onto the stage in dual beam chamber.

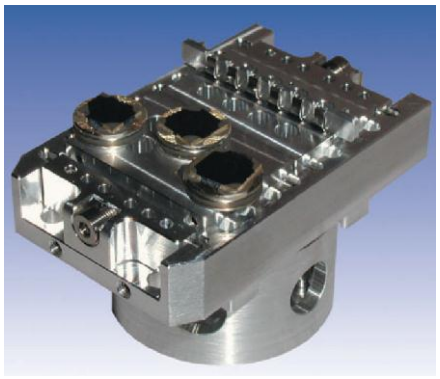

Figure 3.6. Shale Gas Samples Pinned in the Stub Holder

3.2.2.3 Perform in situ preparation using dual-beam. Once the specimen stub was pinned in the dual-beam stage and the chamber was vacuumed, the electron beam current and voltage were optimized for imaging. A flat surface spot was selected, and the stage was tilted 52° for milling. To protect the target area from damage, a layer of Pt

(Platinum) measuring 10×10×1.5 µm was deposited on the target area by sputtering as shown in Figure 3.7. This process took approximately 18 minutes. Furthermore, deposition of Pt helps to reduce the curtaining artifacts.

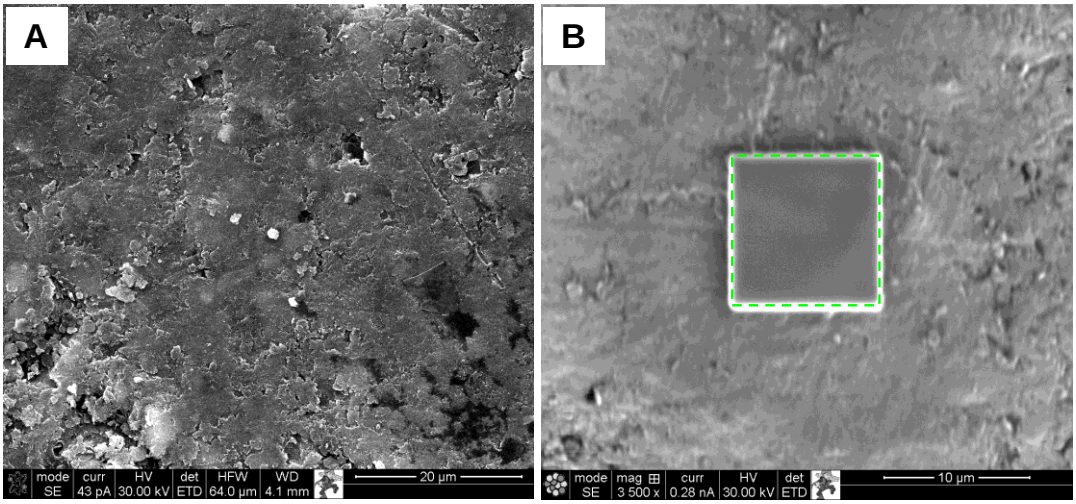

Figure 3.7. Platinum (Pt) Deposit on the Target Area
(A) Flat Surface of the Polished Sample is Allocated, and (B) A 10×10×1.5 µm Layer of Platinum (Pt) is Deposited on the Target Area (~18 min)

To ease the serial sectioning and imaging job, a large volume of the rock material was removed from around the covered spot as shown in Figure 3.8. This process consumed as much as one third of the total job time. The swimming pool was milled away and cleaned in two stages: First, a rough cut of a 25×25×20 µm sample was made using regular cross-sectioning at the highest possible current (21 nA) in front of the targeted area, and silicon was applied. This step takes 20−35 minutes, depending on the milled volume and material. Two parallel pits measuring 7×12×20 µm were then milled away using rectangular milling and a 9.3 nA current. This process takes another 30−40 minutes. Next, the surface exposed to the SEM gun was cleaned using a cleaning cross-section tool. Cleaning was performed in several steps, and the milling current was

reduced to 93 pA for each step. This soft cut requires 30-60 minutes. The total preparation time ranges from 3 to 4 hours.

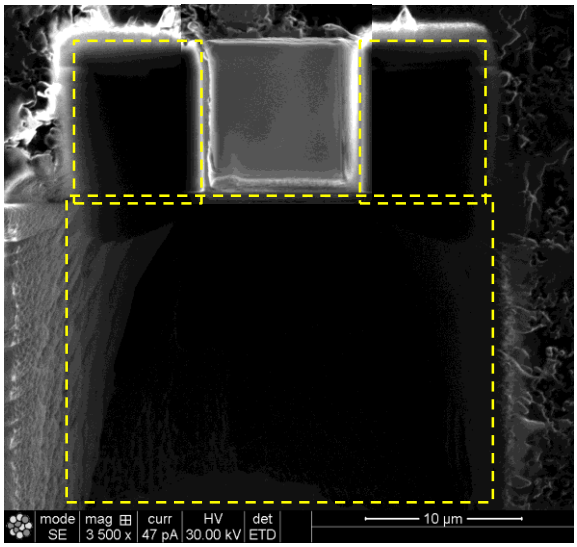

Figure 3.8. Swimming Pool Milling and Cleaning

Some samples suffered from serious curtains and re-deposition of the milled material. To minimize re-deposition, the swimming pool was deepened and widened. Ion beam curtaining is a vexing problem for image stacking. It highly relies on the milled material itself rather than the ion beam focus. Porosity, uneven phase, and platinum deposition are the major factors leading to curtaining in most situations. To diminish curtaining throughout the operation mode, low ion beam voltage (2−5 kV) was exploited. This method reduces curtains thickness to 2 nm. It can also be remedied by utilizing image smoothing algorithms associated with image programs.

3.2.2.4 Perform sequential FIB milling and SEM imaging. Automated and sequential milling process removed 10×0.05×25 µm (12.5 µm3) rock material using 93 pA beam current and gold as an application. Exploiting gold in the milling application results in higher etching rate than using silica applications. After each milling step, a new

two-dimensional surface image was captured by SEM. Each slice takes 4−5 minutes to mill and 30 minutes to obtain high resolution. This procedure was repeated 200 times. The total time required to mill 10×10×25 µm rock sample was between 15 and 20 hours. The process can be speeded up by decreasing the objective milling volume or by increasing the milling beam current. Here, this task was accomplished using an automated program to ease the job. Figure 3.9 illustrates the serial sectioning process.

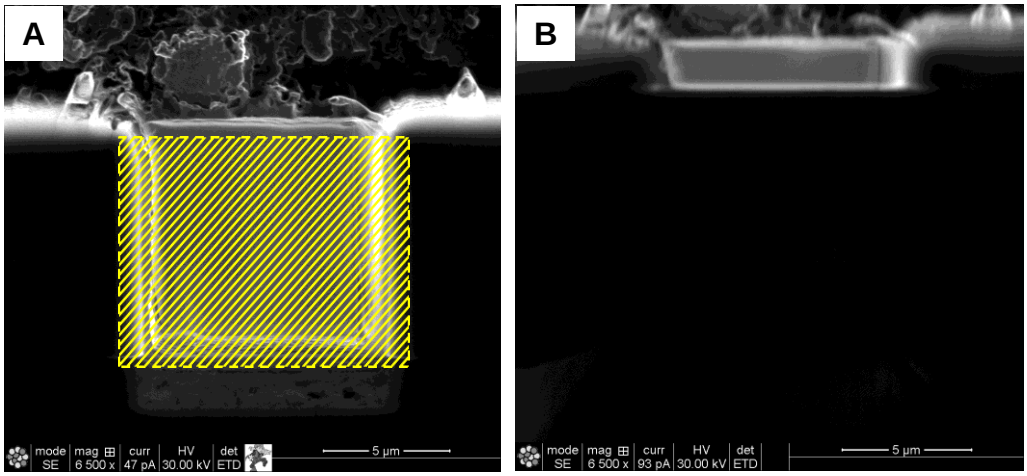

Figure 3.9. Dual-beam Serial Sectioning
(A) Automated Slicing of a 10×0.05×25 µm Area is Performed and 200 Slices are Imaged Sequentially (19−20 hrs), and (B) SEM Image Captured after Finishing Sequential Milling Job

3.2.3. Imaging Results and Discussion. Shale gas has a complex pore structure that cannot be addressed by conventional core analysis. Figure 3.10 shows examples of micron- and nano pores of Utica shale after the swimming pool has been milled and cleaned. Intergranular pore sizes ranged from 15 to 50 nm. Another type of porosity, classified as intraparticular or mineral porosity, occurs within the clay minerals. Its pore opening throat is about 5 nm. The streaks in image (B) are due to charging.

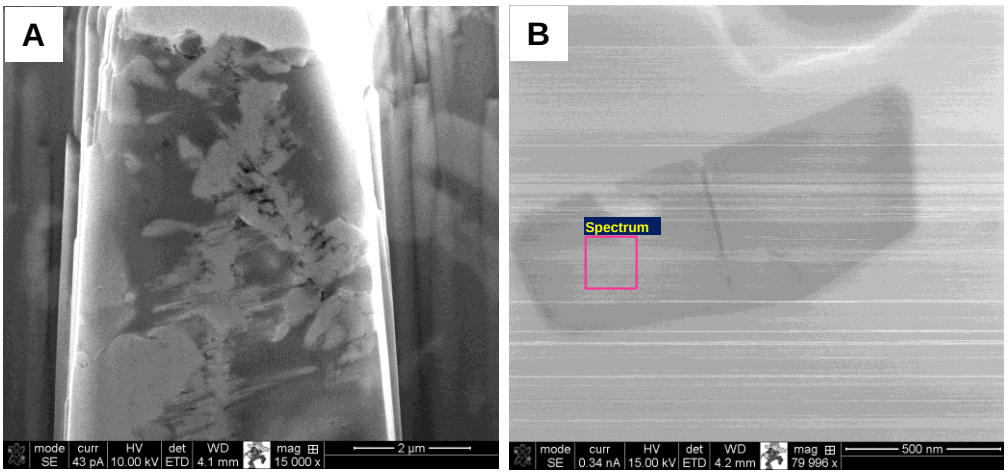

Figure 3.10. SEM Image of Utica Shale Sample No. 3 Dolgeville Fm. Sample, at a Depth of 4,878 ft: (A) SEM Cross-Section Image Shows Pores within the Quartz Grains, and (B) Close-Up SEM Image of Interparticular Porosity

Element analysis using Energy-Dispersive X-ray Spectroscopy (EDS) detector can analyze the captured spectrum of the grain in the image (B) in Figure 3.10. Figure 3.11 presents the EDS spectrum analysis of image (B) in Figure 3.10. The black phase in the middle of the SEM image suggests the existence of pyrite mineral, because it results in a darker color phase, which indicates a higher atomic number and element spectrum confirms the presence of both iron and sulfur. However, since there is no clear relationship between atomic number and phase brightness for the secondary electron image, this dark phase was most likely caused by faster milling rate during the milling process. They were in slight recess compared with the bright phase. Although the silicon spectrum is high and quartz is very common in shales, it is probably from the result of deep x-ray beam penetration. Calcite may be present because natural fractures, which are healed by calcite, have been observed in Utica shale samples. Gallium results from the ion beam source and should be disregarded. The atomic percentage in the spectrum is standard-less.

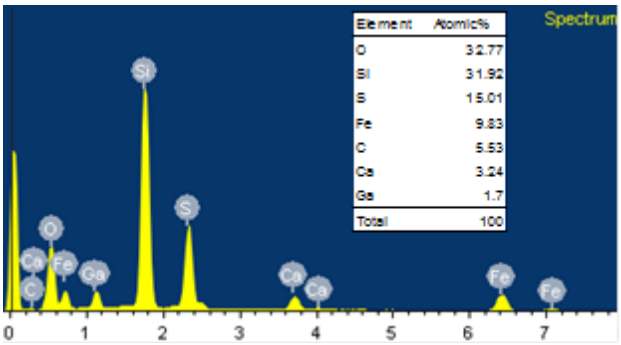

Figure 3.11. EDS Analysis of Clay Mineral Present in Utica Shale Dolgeville Fm. Sample, at a Depth of 4,878 ft

Another SEM images of Utica shale show clay platelets within the quartz grains which create inextricable structure with a variety of pore sizes as presented in Figure 3.12. Diagenesis in shale gas rocks creates a complex mineral structure. Image (B) of the same figure was captured on a freshly fractured surface. It represents shale organic matter (kerogen) and suggests a complex pore structure. It provides plenty of spaces to store adsorbed gas. The morphology and genesis of these nanopores in the organic matter are believed to control the permeability pathways of gas flow (Loucks et al., 2009). Elemental composition analysis affirms the presence of carbon matter. The pores are configured in three dimensions. To characterize such a pore structure, serial sectioning process and three-dimensional pore modeling is required.

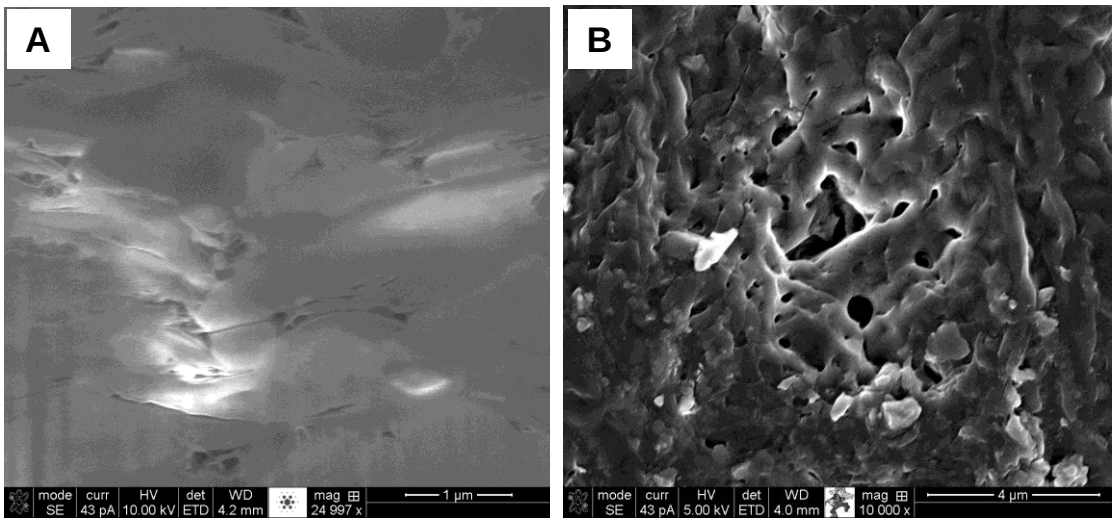

Figure 3.12. SEM Image of Utica Shale Sample No. 2
Indian Castle Fm. Sample, at a Depth of 4,649 ft: (A) Structural Pores of Various Sizes Apparent after Milling, and (B) Organic Matter with A Complex Textile of Pores

Other features of Utica Shale were observed on a freshly fractured surface as shown in Figure 3.13. Clay platelets are closely packed together and form a variety of micron and nano pores (< 2 µm in diameter), as presented in images (A and B). Iintercrystalline pores are also present within the pyrite framboids crystals as shown on image (C). Pyrite framboids micromorphological features that consist of pyrite crystals bound together. These structures provide a porous body. The pore sizes in this mineral are between 20 and 100 nm. Image (D) is a BSE backscattered that clearly reduced the bright spots caused by high electron beam current charges on the target surface.

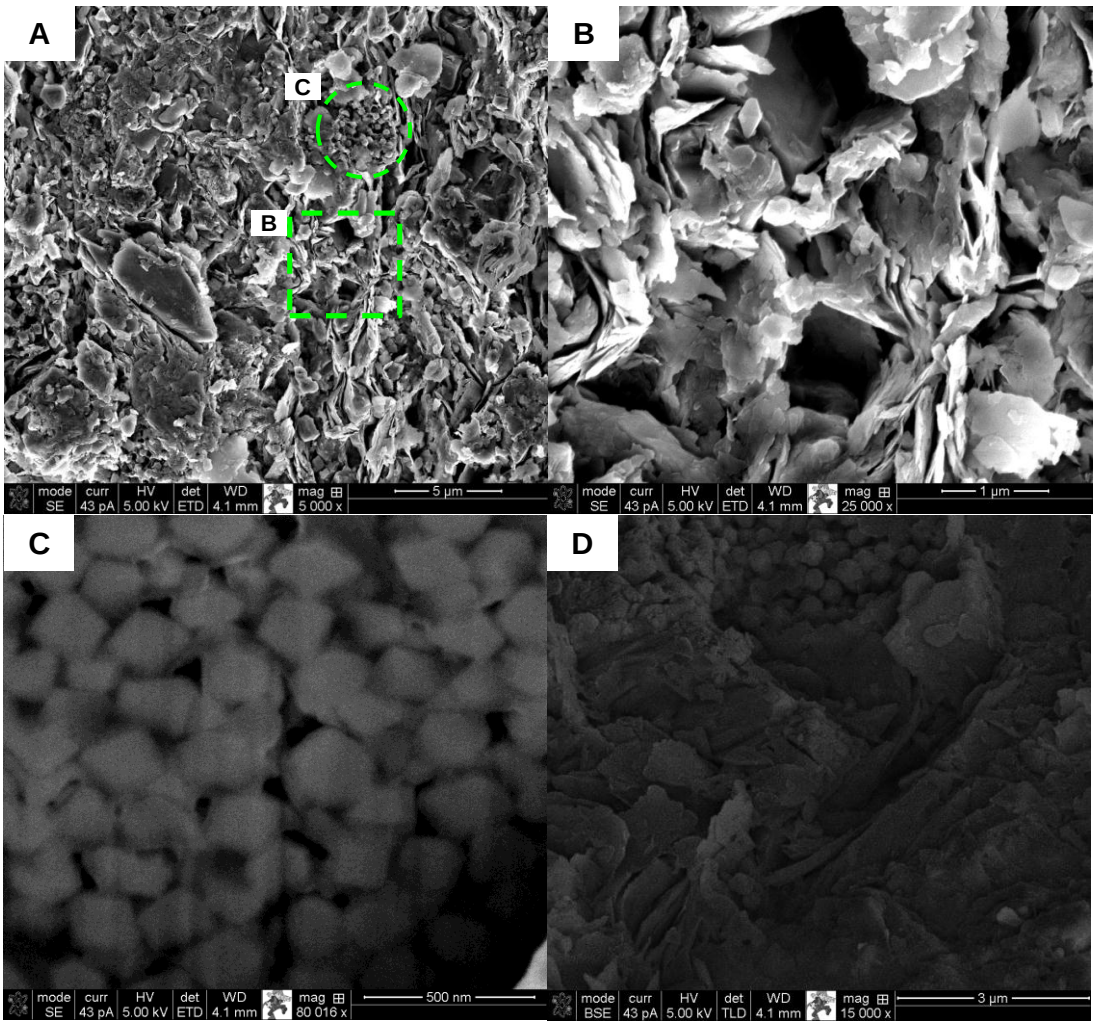

Figure 3.13. SE/BSE Images of Utica Shale Sample No. 2 Indian Castle Fm. Sample, at a Depth of 4,649 ft: (A) Fresh Surface Shows Clearly Different Clay Structure of Pyrite Framboids and Clay Platelet, (B) Zoomed-in Micro- and Nano-pores, (C) Nano-porosity is Observed within Pyrite Framboids and (D) BSE Image Confirms Pyrite Framboids Surrounded by Clay Platelet

Element analysis using the spectrum generated by the EDS detector confirms the existence of pyrites, in addition to other clay minerals as shown in Figure 3.14. This figure presents full spectrum map of Utica shale sample no. 2 that suggests the existence of abundant minerals such as pyrite, illite, quartz and some calcite.

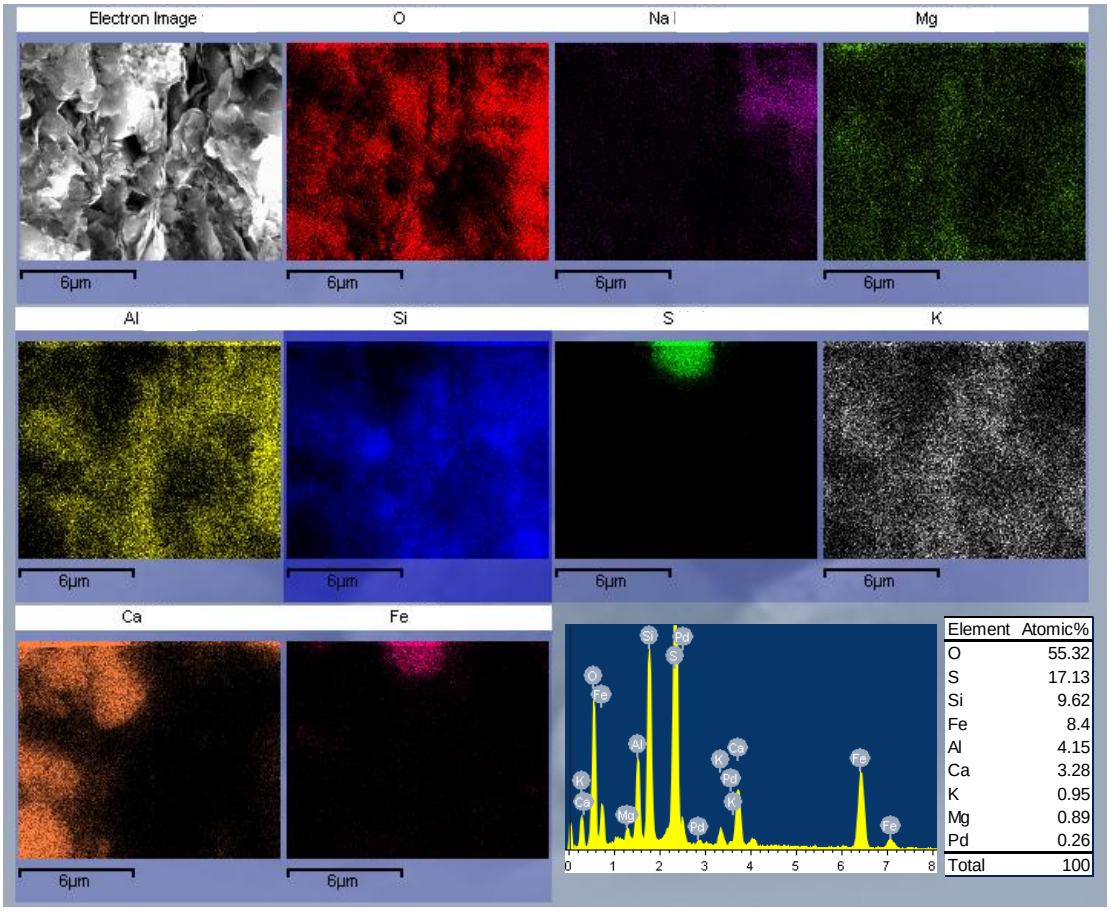

Figure 3.14. EDS Element Mapping Results of Utica Shale Sample No. 2

Pyrite framboids are clearly seen in Figure 3.14 where they are compositionally pyrite mineral (FeS_2) but they are roughly spherical aggregates of discrete equi-regular euhedral microcrystallites of around 0.25 µm in diameter, with the average aggregate size ranging from 5−20 µm. Illite is a very common clay mineral in gas shale source rock. It is compositionally class of aluminum silicates but structurally complex with wide range of properties. It is considered as non-swelling clay and has low cationic exchange capacity (CEC). Quartz is the second most abundant mineral in shale after clay minerals. Element mapping shows about 10% silicate exists in Utica shale. Calcite is a common mineral in the most Utica shale samples where it can be named as calcareous shale indicating high quantity of lime. XRD results section shows only Indian Castle sample from Utica shale exhibits less counts of calcite than samples acquired from Dolgeville formation.

Fayetteville shale sample exhibits three main features which can be seen on the SEM image of the milled surface as illustrated in Figure 3.15. First, a vuggy porosity which is marked in spot (A) with 2−8 μm pore size offers a sizable storing space for free gas. Second, a porous kerogen is shown on image (B) which contains abundance of nano pores with size of 5−100 nm. Third, cluster of conductive natural fractures on image (C) shows opening size of 25−50 nm. The curtaining in this case is most likely due to the material itself and high ion beam milling voltage (30 kV).

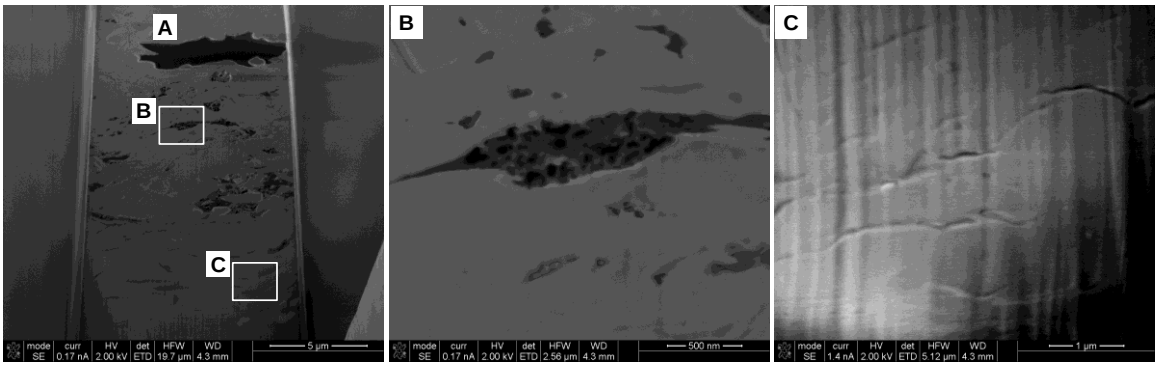

Figure 3.15. SEM Images of Fayetteville Shale Sample
(A) Vuggy Micro-porosity, (B) Kerogen Nano-porosity Occupies about 40−50% of the Organic Matter, and (C) Nano Natural Fractures

Fayetteville shale samples have shown the highest content of the total organic carbon (TOC) compared to Utica and Haynesville shale samples. The extracted TOC value from the previous 2D SEM image shown in Figure 3.15 is 3.91%. It highly matches the obtained TOC from conventional geochemical analysis which was 4.04 wt. % (Elgmati et al., 2011). This method may be used for future studies as an alternative way for measuring TOC content in shale gas rocks. It is fast and relatively inexpensive. To confirm kerogen entity, element analysis is performed and resulted in high carbon spectra between 37−42% as shown in Figure 3.16. Element anaylsis was performed at three positions. According to the spectrum counts, the dark porous spots represent kerogen

matter which contains high carbon content. Meanwhile, the solid part is believed to represent aluminum silicate class mineral (possibly illite).

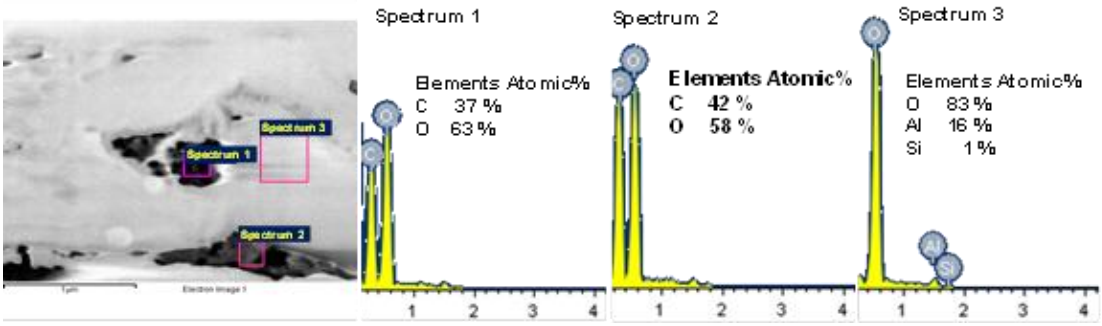

Figure 3.16. EDS Spectrum Analysis of Fayetteville Shale Sample Spectrum 1 and 2 Confirm Kerogen Presence, and Spectrum 3 Represents Aluminum Silicate (clay)

3.3. 3D SUBMICRON PORE NETWORK RECONSTRUCTION

3.3.1. 3D Volume Reconstruction Procedure. After performing serial sectioning and sequential imaging of 200 images from the Fayetteville shale sample, all the two-dimensional SEM images were stacked into three-dimensional pore structural model. The process was performed into two main steps. Commercial imaging softwares (Avizo Fire 6.3 and ImageJ 1.4) were used for reconstructing the three-dimensional model and obtaining and visualizing advanced qualitative and quantitative information from the shale gas SEM images.

The first step is achieved by creating a 2D SEM model of the kerogen nanopores. This was then translated into a 3D model. Figure 3.17 illustrates the 2D binary image conversion. The original image (A) was converted into binary image (B) with pixel values of 0 and 1. This was done in order to measure the nanopores of organic matter. A scale transformation from pixels into micrometers was performed according to image size and magnification scale. A two-dimensional quantification module was utilized to handle

the quantitative analysis of kerogen pore size calculation. However, this algorithm also works for micron-sized pores and fractures within the shale body.

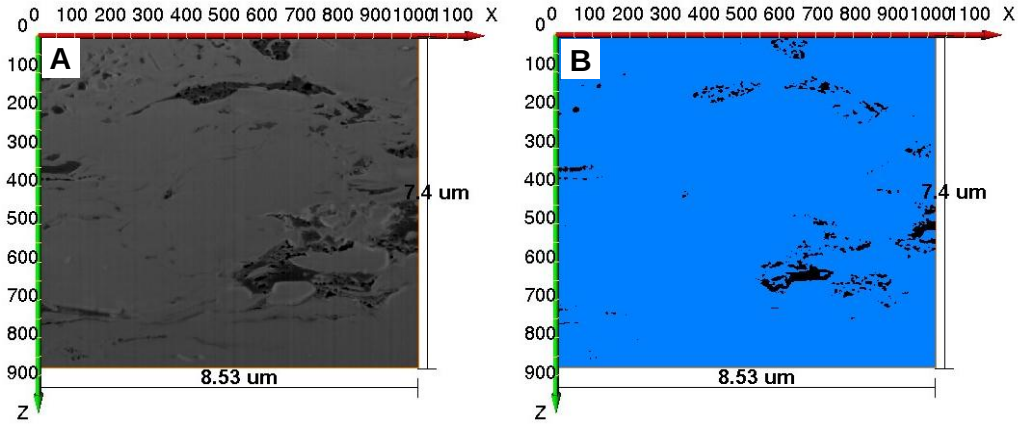

Figure 3.17. Two-dimensional Kerogen Pore Model of Fayetteville Shale (A) SEM Images Showing the Porous Organic Matter, and (B) Converted 2D Binary Image of 0 and 1 Pixel Values

The second step, before stacking the images, involved the alignment process that was done at a marked feature on the image in order to eliminate the mechanical and beam drifts. Then, 200 slices were loaded into a three-dimensional bounding box. A representative elemental volume of 8.85×8.65×9.62 μm was extracted from the bounding box. It is believed that the representative elemental volume is able to provide key insights into the petrophysical properties of the shale gas sample. Optional smoothing and filtration algorithms may be applied if required. Image voxels were converted into a meaningful scale (μm) by taking into account of the original image's magnification scale. Figure 3.18 demonstrates the 3D binary image conversion and separation of Fayetteville shale gas sample. The conversion and separation were also required within the chosen voxel thresholds. They were performed using some quantification modules that are associated with the stacking software. It is used to determine grain element boundaries for defining the micro-structural pores of shale gas samples.

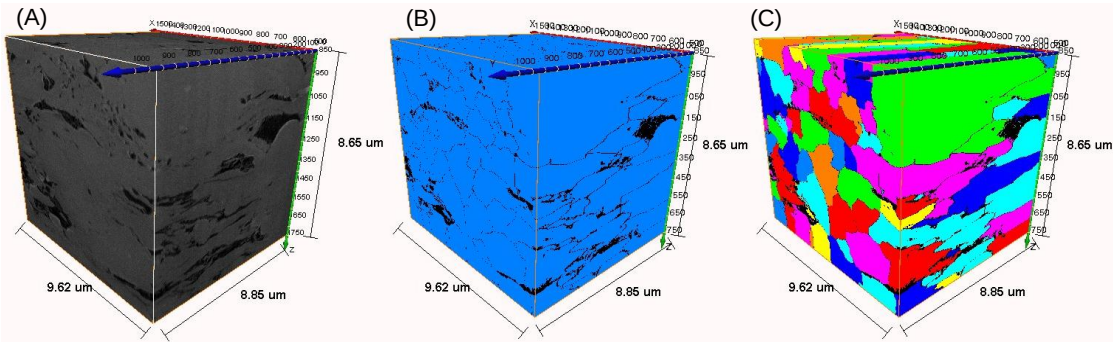

Figure 3.18. Three-dimensional Reconstructed Pore Model
Fayetteville Shale Sample: (A) 200 Slices of Two-dimensional SEM Images are Aligned and Stacked, (B) Converted Three-Dimensional Stack to Binary Image of 0 And 1 Voxel Values, and (C) Element Boundaries are Determined and Labeled To Perform the Porosimetry Analysis

Once all the previous steps are carried out, an analysis module is used to perform statistical analysis and to calculate rock pore size distribution according to the chosen separation algorithm.

3.3.2. Structural Pore Size Results and Discussion. Pore sizes and pore-size distribution in the grains of inorganic and organic matters were determined by using a computer software (Avizo Fire 6.3) to outline and measure all individual pores in an area of interest. Pore diameters were determined for each pore, and median diameters were determined for groups of pores.

The resulted histogram of two-dimensional SEM model is shown in Figure 3.19. It presents micron-sized pores of 2 μm as the major pores. The extracted rock porosity is 3.34% and kerogen porosity occupies about 40−50% of organic matter. Kerogen nanopores are between 10−50 nm. The computed kerogen permeability is 4.76×10^{-4} md according to Kozeny equation by using average pore throat diameter of 30 nm. It is suggested to develop new technology which is capable to extract the adsorbed and free gas from the very tight pores through the macro hydraulic fractures. This definitely will maximize the unconventional gas reserve from shale gas plays.

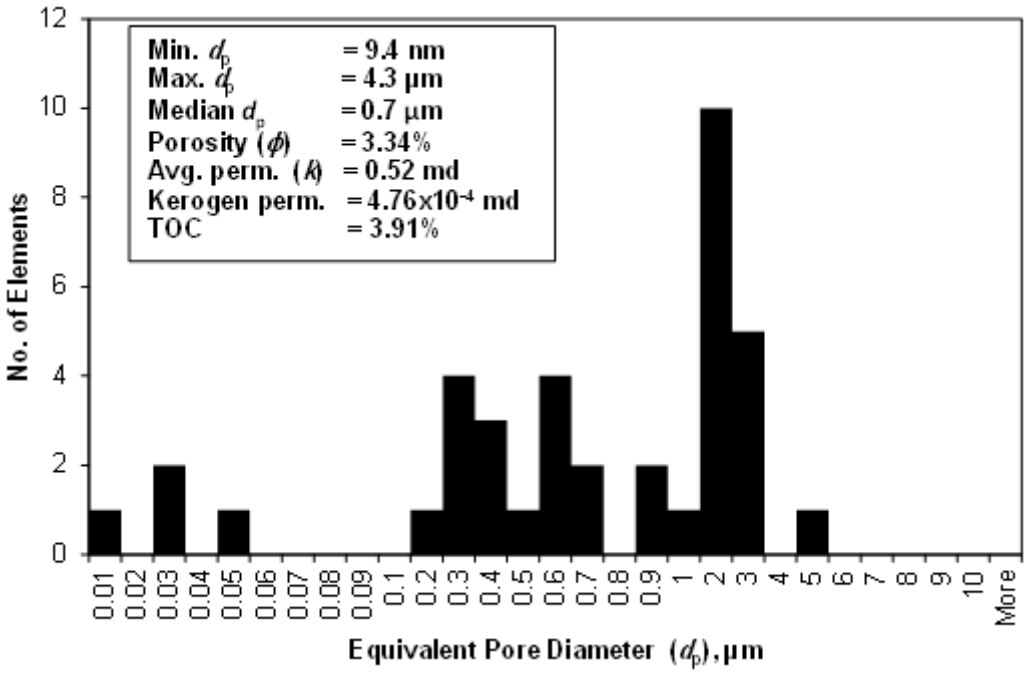

Figure 3.19. 2D Kerogen Pore Size Histogram

The 3D volume pore distribution analysis is carried out. As seen from Figure 3.20, the major pore size, which corresponds to the highest frequency, is 30 nm. This validates the analysis of 2D kerogen model. Only a small number of micron-sized pores of 3 µm exist in the three-dimensional model. Total porosity of 28.22%, tortuosity of 1.44 and anisotropy of 0.28 were outputted. Moreover, rock permeability is determined by using the adjusted Kozeny equation which takes pores tortuosity into account. Overall rock permeability is 0.01 md. It is slightly higher than other shale samples; however, this might be attributed to the abundance of micro-fractures or the vuggy porosity.

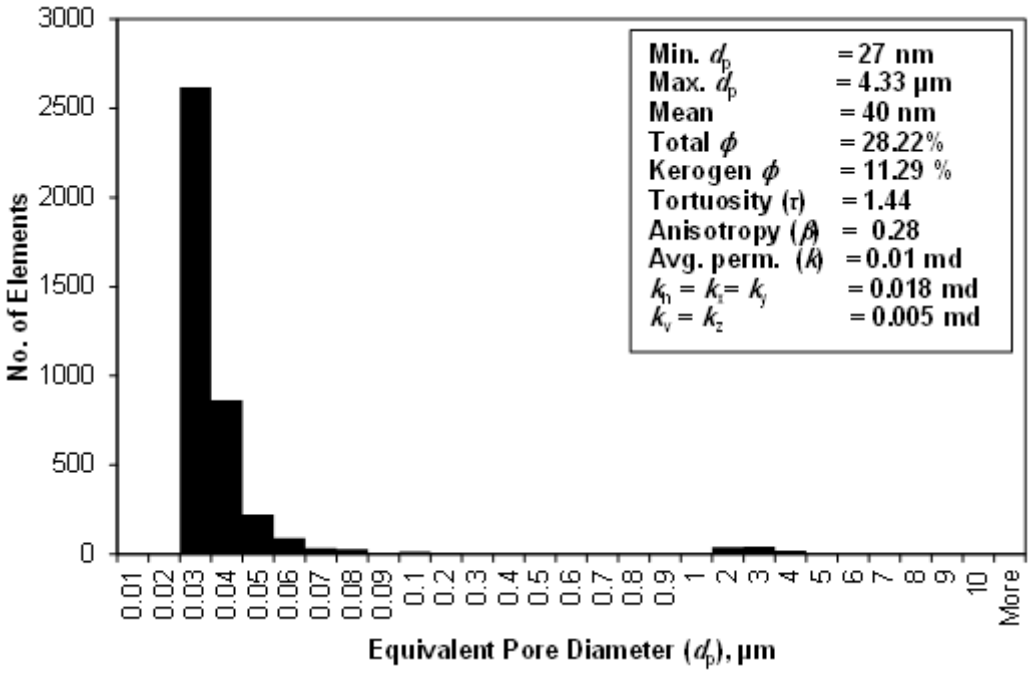

Figure 3.20. 3D Volume Pore Size Histogram

Tortuosity coefficient (τ) is basically defined by the ratio of actual flow path (L_a) to the total sample length (L). It is always greater than 1 for heterogeneous rocks. From most rock laboratory standpoint, tortuosity can also be defined by the following equation.

$$\tau = \left(\frac{L_a}{L}\right)^2 \tag{3}$$

Using anisotropy definition of vertical to horizontal permeabilities ratio (i.e. $\beta = k_v/k_h$) and assuming that horizontal permeabilities (k_x and k_y) in x and y directions are equal to k_h, both vertical and horizontal permeabilities were determined. The average horizontal permeability is 0.018 md; meanwhile, the vertical permeability is 0.005 md.

In spite of all, submicron pore modeling is believed to be a powerful tool compared to MICP method. It provides direct measurement of the original pore structure and it also defines the bulk pores of the shale sample without any manipulation. Yet, the diagnosis scale is in submicron scale compared to the gigantic scale of the mercury

porosimetry test. In order to make results universal, a comprehensive statistical study is required.

3.4. X-RAY DIFFRACTION AND CLAY MINERALOGY

As known that clay minerals are very fine grained that X-ray methods, rather than hand specimen or optical methods, are used to identify them. Moreover, clay structure is three dimensional and varies considerably from one type of clay to another. X-Ray diffraction is considered to be the best method in defining clay minerals.

3.4.1. Theory of X-ray Diffraction. The principle of X-ray diffraction measurements originated from Bragg's law (1912). A mechanical assembly called goniometer makes up the sample holder, detector and x-ray tube as shown in Figure 3.21.

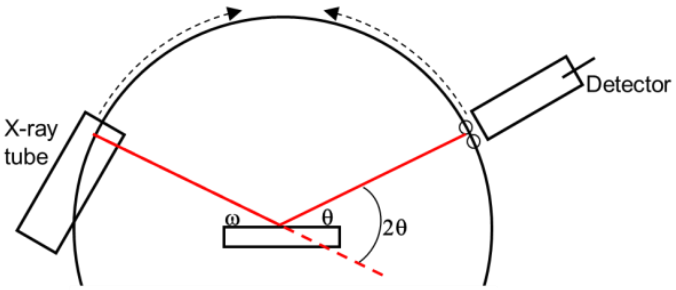

Figure 3.21. XRD Goniometer Sketch

In a θ:θ instrument, the sample is fixed and the tube rotates at a rate -θ°/min and the detector rotates at a rate of +θ°/min. The incident angle, ω, is defined between the X-ray source and the sample. The diffracted angle, 2θ, is defined between the incident beam and the detector angle. The incident angle θ is always ½ of the detector angle 2θ.

Bragg's law (1912) explains the relationship between the incident and detector beams with respect to the examined sample. It can be written as shown below for the use of X-ray diffraction analysis.

$$n\lambda = 2d\ sin\theta \quad (4)$$

where *n* is an integer (i.e. 1, 2, 3…, etc.), λ is the wavelength of the incident X-ray beam (1.54 Å for Copper), *d* is the distance between atomic layers in a crystal, and θ is the angle between the incident ray and the scattering planes. The diffraction planes are 00l= (001), (002), (003), (004). When X-ray radiation passes through matter, the radiation interacts with the electrons in the atoms, resulting in scattering of the radiation. If the atoms are organized in planes (i.e., the matter is crystalline) and the distances between the atoms are of the same magnitude as the wavelength of the X-rays, constructive and destructive interference will occur. This results in diffraction where X-rays are emitted at characteristic angles based on the spaces between the atoms organized in crystalline structures called plane as shown in Figure 3.22.

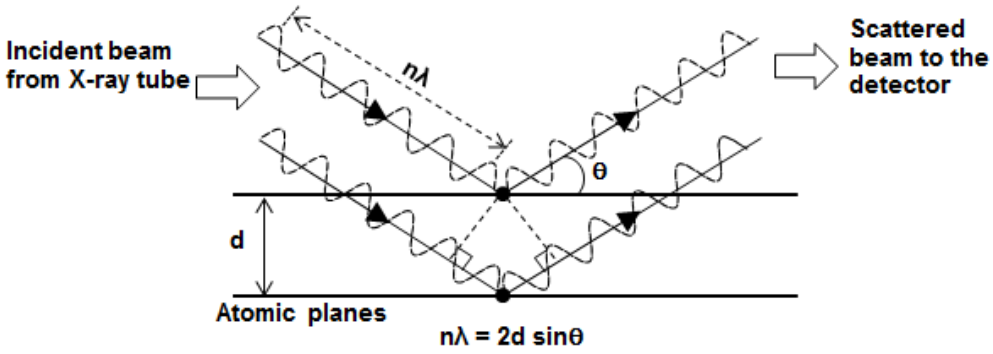

Figure 3.22. X-ray Goniometer Theory Based on Bragg's Law

3.4.2. XRD Test Procedure. Sample preparation for XRD analysis of clay minerals is probably the most critical step. The problem is how to free individual crystallites of clay from the rock or sediment without damaging them in any way, physically and chemically, and then to prepare ordinated mounts that will satisfy the requirements for X-ray analysis. Much has been written on this aspect of analysis, and different authors favor different procedures. Some of these procedures are time-consuming and quite involved; some require equipment that is not readily available.

A good discussion of sample preparation and its problems is found in Moore and Reynolds (1989). Here we are going to adopt a procedure described originally by George S. Austin (New Mexico Bureau of Miners & Mineral Resources) and modified by Dr. David Wronkiewicz, Missouri University of Sciences and Technology. The procedure described below is for identification only; it allows most common clays to be identified but ignores many of the potential problems in favor of simplicity and speed.

(1) The sample is crushed to a fine powder. Unfortunately, this will reduce all minerals to clay size so that they cannot be separated from the clay minerals.

(2) The sample is disaggregated in distilled water. There are several ways to accomplish this. The simplest way is to put 5-25 grams of the sample in a covered vial with distilled water and shake vigorously. If there is flocculation during the next step, then a peptizing agent such as Clagon or NH_4OH is used before agitating.

(3) A clay fraction is separated from the coarser material. If the disaggregated sample is allowed to stand for 10 minutes, the coarse fraction will have settled and the clay and some silt will remain in suspension; longer setting times are required for better separation. The amount of suspended clay depends on the relative volumes of sample and distilled water, and on the amount of clay in the sample.

(4) The clay sample is then mounted on a glass slide. To achieve this step, a pipette or eye dropper to draw off some of the clay-water slurry prepared in step 3 was exploited. The entire glass slide was covered completely with the slurry but without causing it to overflow. Then, the slide was allowed to dry overnight at room temperature.

(5) Finally, the glass slide was brought into θ:θ goniometer for XRD analysis.

The specimens were examined three times on XRD instrument in different circumstances. Sometimes it is difficult to distinguish between chlorite and kaolinite

when only weak peaks are present at 12.5° and 25° 2θ. Such a sample could contain only chlorite, only kaolinite, or a mixture of the two. In this situation, the sample is treated chemically or heated and then reexamined. To eliminate the possibility of any interference between the peaks of different clay minerals, the following procedure is implemented. Initially, the samples were examined before applying any treatment and the resulted run was marked as “Untreated”. Then the samples were put in glycolation vessel for 24 hours to widen clay mineral layers for better mineral identification resolution. This run was called “Glycolated” run. The last run was performed after heating the samples up to 375°C for 1 hour and it was named “Heated” run.

The qualitative identification procedure begins with searching for a mineral that has the strongest peaks, and follows with confirming the choice by finding the positions of weaker peaks for the same mineral. By using basal spacings (d) and 2-theta for Cu K-alpha radiation in Table 3.1, clay and non-clay minerals peaks can be readily distinguished. Some mineral peaks may be invariant because the mineral structure tolerates no significant atomic substitutions. Our focus is at small diffraction angles, because most of the important clay peaks occur at 2-theta values of 40° or less; therefore, theta is 20° or less, and that value is sufficiently small to fit the foregoing argument to a pretty good approximation.

Table 3.1. Basal Spacings (d) and 2θ for Cu K-Alpha Radiation
(Adopted from modified procedure described by George S. Austin-New Mexico Bureau of Miners & Mineral Resources)

Clay Mineral Group	001		002		003		004	
	Å	2θ	Å	2θ	Å	2θ	Å	2θ
Chlorite	14.1-14.2	6.2-6.3	7.05-7.1	12.5-12.6	4.7	18.9	3.52-3.54	25.3-25.1
Kaolinite	7.16	12.4	3.57	24.9	2.38	37.8	1.78	51.3
Mica (Illite)	9.97-9.98	8.8	4.96	17.9	3.32	26.8	2.49	36.1
Ca Smectite	15.4-	5.7	7.7	11.5	5.1	17.4	3.8	23.4
Na Smectite	12.4	7.1	6.2	14.3	4.1	21.7	3.1	28.8
Ca Smectite - glycol	17-	5.2	8.5	10.4	5.7	15.6	4.2	21.2
Na Smectite - glycol	16.7							
Vermiculite	14.1-14.3	6.3						
Non-Clay Minerals								
Calcite		29.5						
Dolomite		30.9						
Quartz		20.8		26.6				
Albite and Microcline		27.7						
Pyrophyllite		9.6		19.3		29.1		

3.4.3. XRD Results and Discussion. Clay minerals are compositionally a class of aluminum silicates, and structurally they are complex with a wide range of properties. The basic building blocks are silica tetrahedral and aluminum octahedral. Carbonate minerals are commonly associated with clay minerals specially calcite and dolomite. Peak positions will vary with the limited solid-solution series between calcite and dolomite.

Yaalon (1962) applied normative calculations on the chemical composition of 10,000 shales and arrived at the following average composition: 60% clay minerals-mostly illite, 20% quartz, 10% feldspar, 6% carbonates, 3% iron oxide, and 1% organic matter. This agrees with the presented XRD results.

Semi-quantitative assessments make the identification of individual minerals in shale gas samples much more valuable. Unfortunately, the intensity of a mineral's diffraction peaks cannot be directly used as an accurate measure of mineral abundance, because different minerals, different atomic planes within a mineral, and different samples of the same mineral do not have the same ability to diffract X-rays (Biscaye, 1965). However, this study uses the modified procedure for semi-quantification of clay minerals with approximate accuracy of ±10%. The computed clay mineral contents were often avoided because of their weak or doubtful peak intensity. Table 3.2 summarizes the semi-quantitative analysis of XRD results for shale gas samples.

Table 3.2. XRD Analysis Summary

Shale Gas Source Rock Samples		Sample No. 1	Sample No. 2	Sample No. 3	Sample No. 4	Sample No. 5
Clay minerals	Chlorite	31%	Low	-	-	-
	Illite	69%	High	V. Low	V. Low	Low
Non-Clay minerals	Calcite	Low	Low	High	High	V. Low
	Dolomite	-	V. Low	-	V. Low	V. Low
	Quartz	Moderate	Moderate	V. Low	V. Low	High
	Albite and Microcline	-	Low	-	-	-

Figure 3.23 presents a combined plot of XRD results for five shale gas samples. Utica shale sample obtained from Indian Castle formation and Haynesville shale exhibit the highest amount of illite whereas the first strongest peak at 8.8° 2θ is obviously seen. Both of the Utica shale samples acquired from Dolgeville formation are classified as calcareous shale. XRD results also suggest high calcite content. Fayetteville shale may compositionally comprise of higher quartz content than illite because illite's peaks intensity is almost vanished.

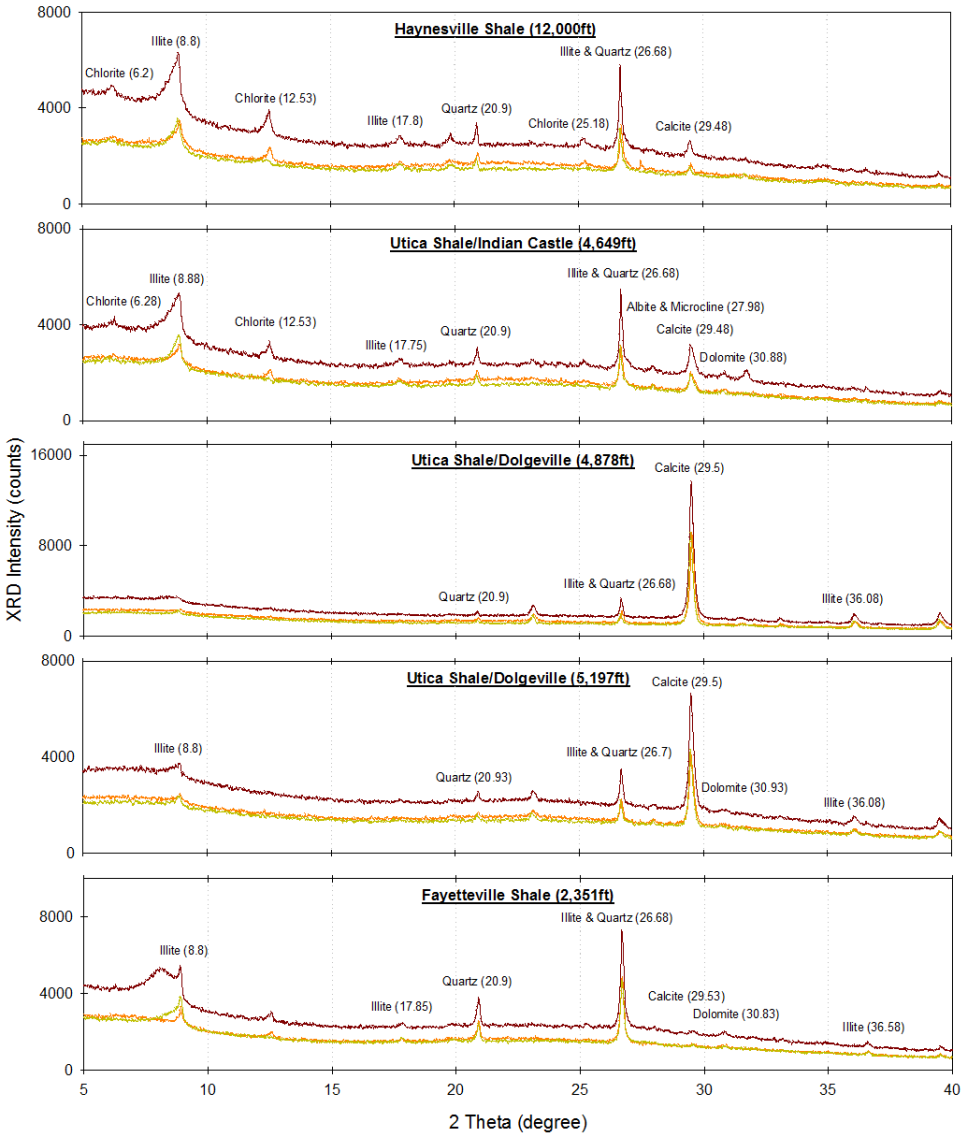

Figure 3.23. X-Ray Diffraction Results of the Five Shale Gas Samples

3.5. CONTACT ANGLE MEASUREMENTS

Shale gas rocks are usually hydraulically fractured in order to be capable to produce gas. Chemical additives such as friction reducers and viscosifiers have often been added into fracturing fluids. However, the additives in fracturing fluids may impair the fracture permeability and alter the rock wettability which influences the gas flow ability. To remedy this problem, intensive study of rock surface and fluid composition

interaction should be performed in order to mimic the gas flow in submicron pores. Gas flow behavior in submicron pores of shale gas is controlled by rock mineralogy, organic matter content and fluid type. Clay minerals are very special and they are different than other minerals. All minerals are electrically neutral except clay minerals, which always negatively charged. They are the only minerals that are capable to exchange cation along the negative surface charges (ions). Therefore, clay minerals have high cation exchange capacity (CEC).

3.5.1. Contact Angle Principle. When only one fluid exists in the pore space, there is only one set of forces to consider; which is the attraction between the rock and the fluid. When more than one fluid phase is present, there are at least three sets of active forces affecting capillary pressure and wettability as presented in Figure 3.24. The three sets of forces are solid-liquid interfacial tension (γ^{sl}), solid surface tension (γ^{sv}) and liquid surface tension (γ^{lv}).

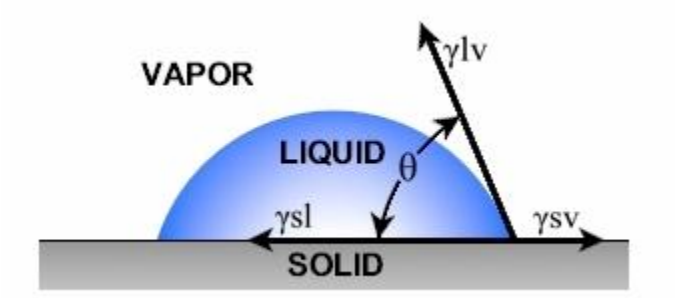

Figure 3.24. Equilibrium of Forces at Liquid-Vapor-Solid Interface

Rock wettability is basically defined by the contact angle measure. The goniometer presented in Figure 3.25 is exploited to measure the contact angle of various fluids on the shale rock surfaces.

Figure 3.25. Contact Angle Goniometer Instrument

The resulted contact angle from goniometer device which uses sessile drop technique is defined by the following equation

$$\theta = 2\ tan^{-1}\frac{2h}{w} \tag{5}$$

where θ is the contact angle, h is the drop height and w is the drop width. Polished plates of shale gas samples were used as representative surfaces for sessile drop and contact angle measurements. In our measurements, the specimen do not account for surface roughness, the material heterogeneity and the presence of organic matter. Alternative wettability measurement methods which are referred by Tiab and Donaldson, (1996) could be one of the best tools for shale gas wettability study.

3.5.2. Wettability Results and Discussion. The obtained contact angle measurements from five shale samples using six chemical additives of fracturing fluid is presented in Figure 3.26. The six additives are comprised from two polymers (e.g. FRW-18 and FRW-20) and four surfactants (e.g. Inflo-45LB, Inflo-250, GasFlo-G, and Flowback-30). The examined solutions were made of 0.1% wt. concentration. The presented results were repeated at least three times for each shale chip.

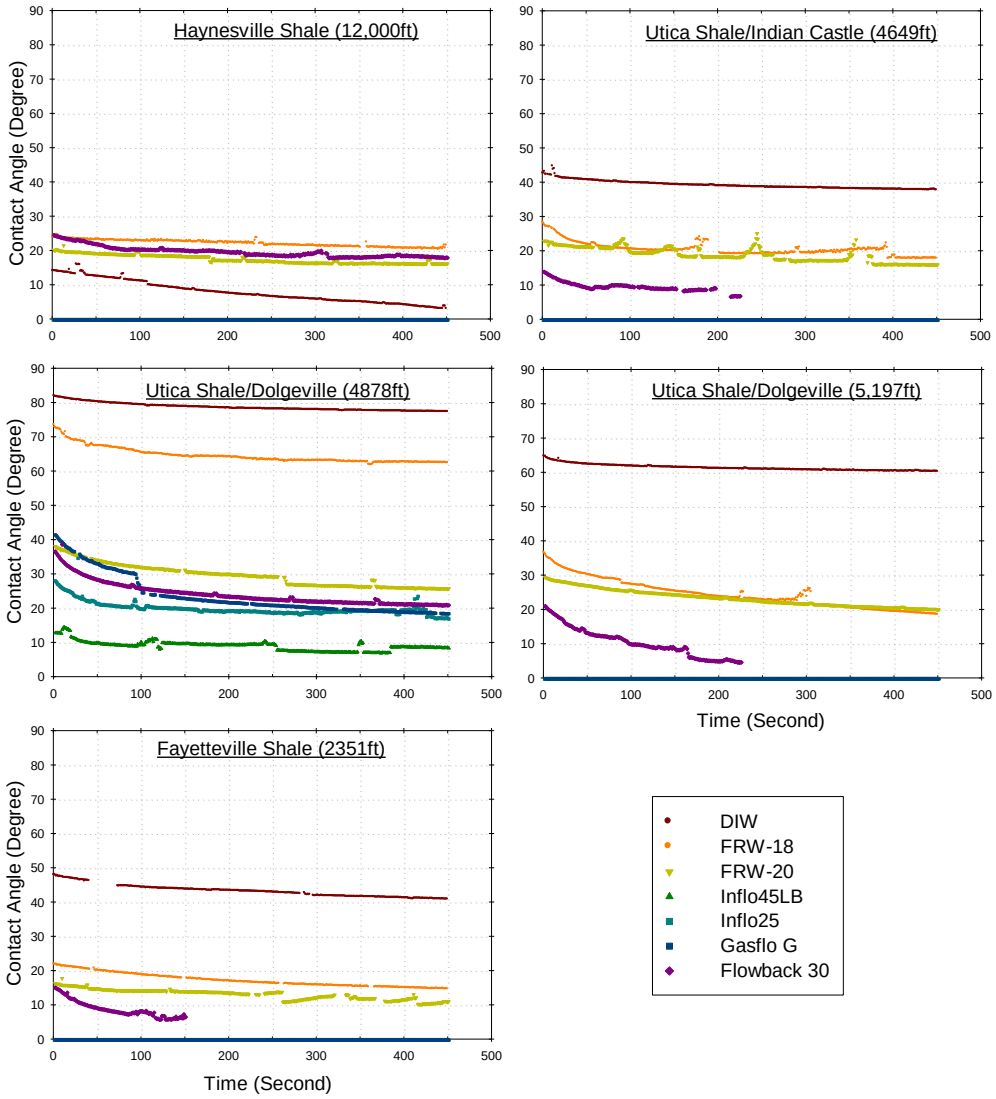

Figure 3.26. Contact Angle Results
Five Shale Gas Samples were Examined Using Six Fracturing Fluid Additives

All contact angle results were compared to deionized water (DIW) contact angle and summarized in Table 3.3.

Table 3.3. Contact Angle Results Summary
Contact Angle Results Have Accuracy of ± 5 Degrees

Shale Gas Source Rock Samples	Sample No. 1	Sample No. 2	Sample No. 3	Sample No. 4	Sample No. 5
DIW	14.0	42.5	81.8	64.6	47.8
0.1% FRW-18	23.8	28.2	73.4	36.5	21.8
0.1% FRW-20	20.4	23.1	38.3	29.6	16.5
0.1% Inflo-45LB	0.0	0.0	13.0	0.0	0.0
0.1% Inflo-250	0.0	0.0	28.2	0.0	0.0
0.1% GasFlo-G	0.0	0.0	41.6	0.0	0.0
0.1% Flowback-30	24.7	14.1	36.8	21.2	15.3

It is highly observed that all the tested fracturing fluid additives on Utica and Fayetteville shale rock samples result in reducing the contact angle and making the shale rocks behave more water-wet like surface compared to DIW contact angles. The scenario for Haynesville shale sample is slightly different, whereas both polymers and Flowback-30 surfactant tend to slightly raise the contact angle to intermediate water-wet level. This might be attributed to (1) very high illite concentration (70%) as illite peak intensity on XRD data suggests and (2) low organic matter content of Haynesville shale (TOC = 0.81 wt. %) as reported by Elgmati et al. (2011).

Utica shale samples acquired from Dolgeville formation result in the highest DIW contact angle which is between 60−80°. This rock behaves like oil-wet material. X-ray diffraction results suggest high concentration of calcium carbonate (calcite). However, Utica shale sample acquired from Dolgeville formation at depth 4,878 ft behaves slightly different when it is treated with all surfactants and polymer FRW-20. These solutions have high tendency of altering wettability of this rock to water-wet with contact angle of 10−30°. Polymer FRW-18 impairs this surface wettability toward water-wet very slightly. This is attributed to fracturing fluid chemical composition and clay mineralogy. It is noted that this sample is classified as calcareous shale sample and sometimes it is

also called carbonate-like shale. This rock sample is very hard to saw. It is likely attributed to (1) very high lime content as calcite peak intensity in XRD results suggests and (2) extremely low organic matter content (TOC = 0.31 wt. %) as documented by Elgmati et al. (2011). According to Leverson (1954), Perrodon (1983) and Wang and Reed (2009), organic substances are oil wet.

In the most presented cases, surfactant solutions alter shale wettability to strongly water-wet system except surfactant Flowback-30 which behaves like polymers. Both polymer solutions alter the wettability of shale gas rocks in the same manner with resulted contact angle of 20−30° except Utica shale sample acquired from Dolgeville formation at depth of 4,879 ft. For this shale sample, only polymer FRW-18 results in high contact angle of 62°.

To sum up, shale gas wettability changes to oil-wet when high concentration of calcite exists. Organic matter content governs fracturing fluid wettability alteration. Low organic matter content would have tendency to change wettability of calcareous samples to oil-wet system.

4. SHALE GAS PALYNOFACIES ANALYSIS

In the present study, palynofacies analysis was carried out on five samples recovered from the Haynesville, Utica and Fayetteville shale-gas source rocks in order to evaluate their kerogen type and degree of thermal maturation. Three of the five studied samples are from the Utica Shale (two samples from Dolgeville member and one sample from the Indian Castle Member), while the fourth and fifth samples are from Haynesville and Fayetteville shales. The data obtained were used to qualitatively estimate some key organic geochemical parameters such as vitrinite reflectance (R_o %) and numerical thermal alteration index (TAI). Samples were also analyzed for TOC content in order to fully understand their source potential.

4.1. METHODOLOGY

Conventional palynological processing technique was used to extract the organic matter (kerogen) from the samples. This included crushing about 10−15 grams of the sample in a mortar to the powder size. Samples were then treated with concentrated hydrochloric acid (HCl) for about 24 hours in order to remove their carbonate content. After neutralization, the silicate fraction in the samples was then dissolved by concentrated hydrofluoric acid (HF) treatment for about 72 hours. Thereafter, samples were washed and sieved to remove clay particles and concentrate organic matter. Only kerogen particles that range in size between 10−106 μm were retained to make the final microscopic slides. Slides were then microscopically examined in transmitted light using variable magnification powers for analysis and photomicrography. A total of 500 kerogen particles were counted from each slide. Particles were classified into four main categories namely, structured phytoclasts, degraded phytoclasts, opaques, and palynomorphs. All slides and residues are housed in the Palynology Laboratory at Missouri University of Science and Technology.

4.2. RESULTS AND DISSCUSION

4.2.1. Kerogen Type. Kerogen is the dispersed sedimentary organic matter that is resistant to the mineral acids hydrochloric acid (HCl) and hydrofluoric acid (HF) (Tyson, 1993). The classification of kerogen type by Tyson (1993) for routine source rock evaluation was used in the present study, in which kerogen type IV (inert material) was identified from all the studied samples, although they differ in the percentages of individual kerogen components. Kerogen type IV was described by (Peters and Cassa, 1994) as dead carbon, which has little or no hydrocarbon generating capability. It is important to mention, however, that the examined samples (except sample #3 from Utica Shale) likely initially contained kerogen type III (gas prone material) that converted to type IV during the process of thermal over maturation.

The sample from the Haynesville Shale contained abundant very dark brown structured phytoclasts and black opaques in association with frequent very dark brown degraded phytoclasts as shown in Figure 4.1. Palynomorph-like particles were observed, but could not be confirmed due to their high degree of degradation and very dark color; hence they were counted as phytoclasts. Equant phytoclasts and opaque particles were much more common than lath shaped ones.

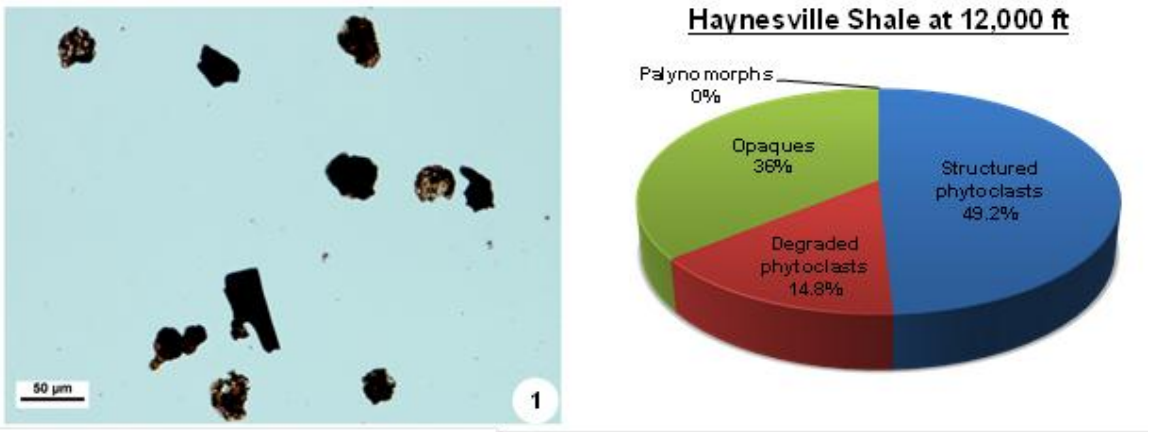

Figure 4.1. Kerogen Percent Distribution and Photomicrograph of Sample #1 Haynesville Shale Sample (Phytoclasts and Opaques are Predominant Kerogen Components)

Figure 4.2 represents the kerogen components that were observed in the shale sample obtained from the Indian Castle Member of the Utica Shale. It shows high abundance of dark to very dark brown structured phytoclasts in association with common black opaques and frequent very dark brown degraded phytoclasts. Palynomorphs (essentially chitinozoans) were very rare and very dark brown to black in color. Many of them were broken down.

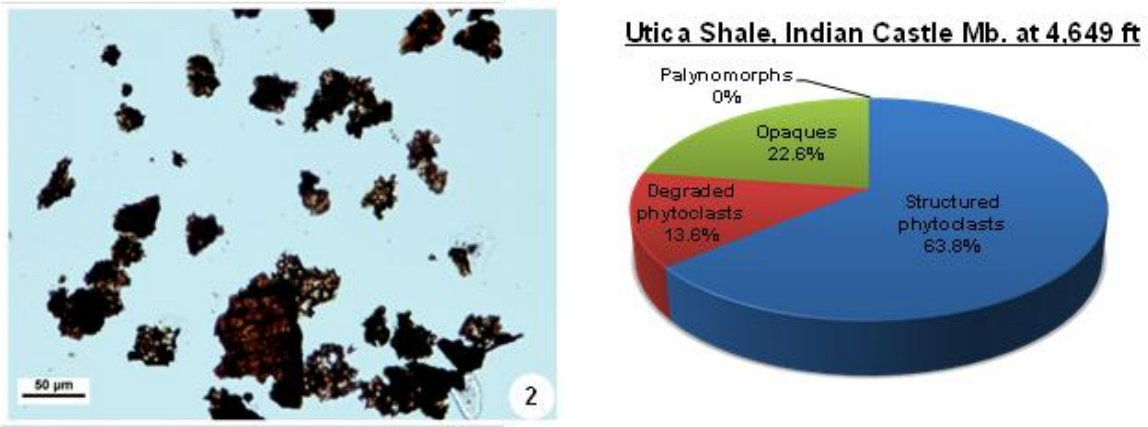

Figure 4.2. Kerogen Percent Distribution and Photomicrograph of Sample #2 Utica Shale Sample from Indian Castle Member (Structured and Degraded Phytoclasts are Predominant Kerogen Components)

Samples from the Dolgeville member of the Utica Shale were not similar in their kerogen composition. The first sample at the depth of 4,878 ft, revealed an overwhelming abundance of black opaques with rare dark brown structured phytoclasts as shown in Figure 4.3. The majority of opaque particles were equant in shape and smaller in size than those recovered from other samples. Very rare palynomorphs were spotted (also essentially chitinozoans) and they were very dark brown in color and extremely degraded and/or broken down.

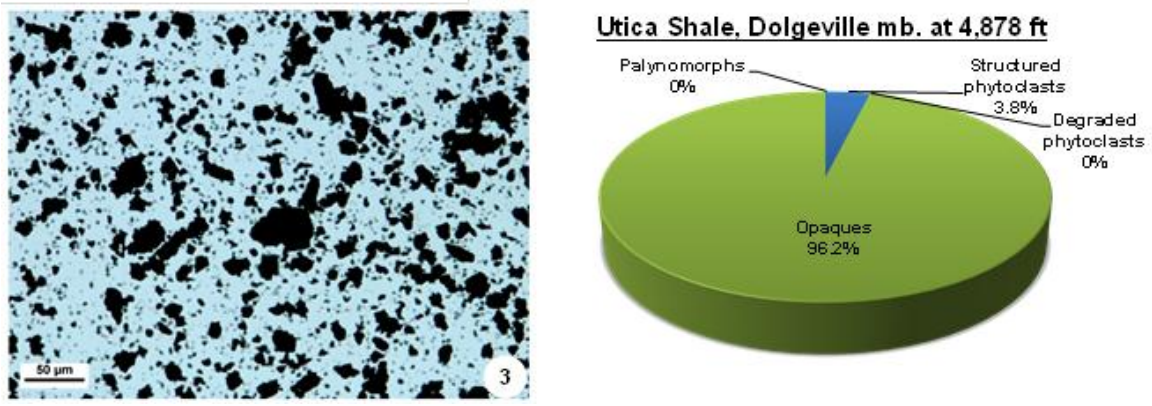

Figure 4.3. Kerogen Percent Distribution and Photomicrograph of Sample #3 Utica Shale Sample from Dolgeville Member at the Depth of 4,878 ft (Opaques are Predominant Kerogen Components)

The second sample of Dolgeville member at the depth of 5,197 ft, on the other hand, contained high abundance of very dark brown degraded phytoclasts along with common black opaques and frequent dark to very dark brown structured phytoclasts as illustrated in Figure 4.4. Palynomorphs were very rare compared to the total kerogen composition. Palynomorphs (essentially chitinozoans) were highly degraded and very dark brown to black in color.

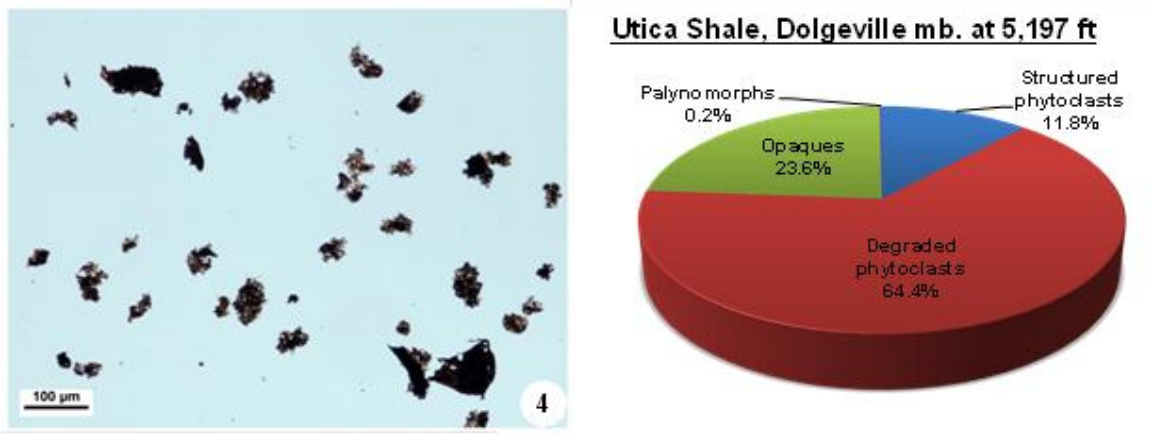

Figure 4.4. Kerogen Percent Distribution and Photomicrograph of Sample #4 Utica Shale Sample from Dolgeville Member at the Depth of 5,197 ft (Degraded Phytoclasts are Predominant Kerogen Components)

The fifth shale gas sample acquired from Fayetteville Shale play had very high abundance of black opaques in association with very little structured and degraded phytoclasts as presented in Figure 4.5. No palynomorphs were observed during the counting process. Almost all of the kerogen particles in this sample were equant in shape.

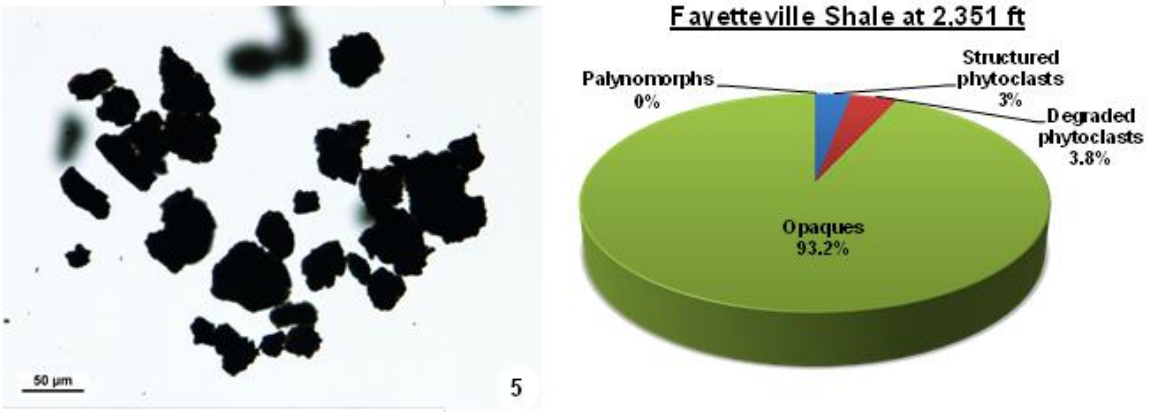

Figure 4.5. Kerogen Percent Distribution and Photomicrograph of Sample #5 Fayetteville Shale Sample (Opaques.are Predominant Kerogen Components)

4.2.2. Thermal Maturation. Thermal maturation is the chemical change induced by post-depositional heating over time that transforms sedimentary organic matter into hydrocarbon (Peters and Cassa, 1994; Traverse, 2007). Color changes in the exine of fossil palynomorphs (e.g. spores and pollen) have long been used to interpret the degree of thermal maturation of potential source rocks.

In the present study, colors of the pseudochitinous walls of chitinozoans and the exine of palynomorph-like grains (gymnosperm pollen?) recovered from the Utica and Haynesville shale gas samples, respectively were examined in order to visually estimate their thermal maturation. The sample from Fayetteville Shale was excluded, since no palynomorphs were observed.

All palynomorphs in the examined samples were dark to very dark brown in color, sometimes even black, implying high level of maturation (i.e. post-mature source rocks) as depicted in Figure 4.6. This denotes that the organic matter have already generated the hydrocarbons respective to their kerogen type. This signifies that the shale gas sample from Dolgeville member at the depth of 4,878 ft (inert kerogen material) has generated little dry gas, or nothing, while those of other samples (with initial kerogen type III content) have generated wet gas and condensate (cf. Batten, 1980). Since all the samples currently contain thermally post-mature type IV kerogen, their source potential is limited to minor amounts of dry gas, or barren, at the present time.

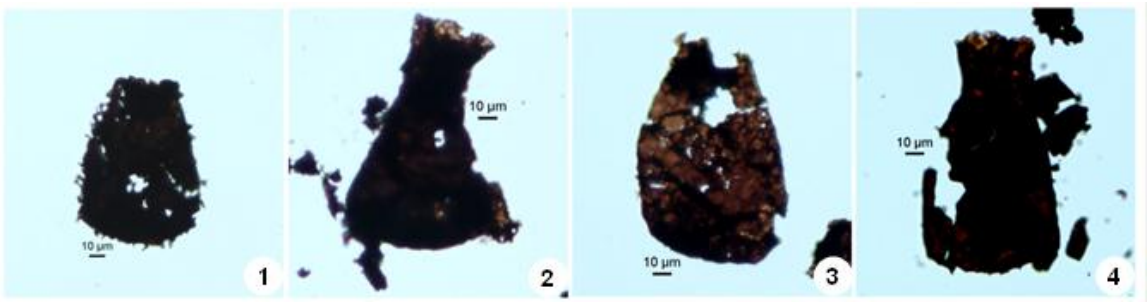

Figure 4.6. Photomicrographs of Some of the Chitinozoan Specimens Identified from Utica and Haynesville Shale Gas Source Rocks

4.2.3. Geochemical Parameters. The aforementioned data about kerogen composition and thermal maturation has been employed to qualitatively estimate some key geochemical parameters, such as numerical TAI and vitrinite reflectance (R_o %). The dark to very dark brown colors of palynomorph walls in the studied samples (excluding Fayetteville Shale sample), which are typical post-mature source rocks, correspond to 4- to 4 TAI and ~1.5−2.5% vitrinite reflectance. This further suggests that these source rocks are mainly in the metagenesis thermal alteration stage (dry gas zone) indicative of about 150−200° C temperature range (Peters and Cassa, 1994).

4.2.4. Total Organic Carbon. The studied samples were sent to the Stable Isotope Mass Spectrometer Laboratory in the Department of Geological Sciences at the University of Florida for quantitative TOC analysis. Samples were grounded and weighed into tin capsules and combusted in a Carlo Erba EA at 1000° C to measure the total carbon content. Samples were then weighed out again into exetainer tubes and acidified with an AutoMate Prep Device. Evolved CO_2 was measured using a UIC 5011 coulometer in order to calculate the total inorganic carbon. TOC is the weight percentage of the difference between total carbon and inorganic carbon.

When interpreting TOC data, circumspection should be considered because it is not a direct measure of hydrocarbon source potential. Instead, a combination of several proxies in addition to TOC must be considered (e.g. lithologic composition, sedimentation rate, kerogen type, thermal maturation, basin redox conditions, etc.).

The analyzed samples have TOC contents of 0.31−4.04 wt. % as shown in Figure 4.7. It is strongly possible that these rocks have once held more TOC content that has decreased over time through the process of thermal maturation and hydrocarbon generation and expulsion. Therefore, it is likely that most of the TOC, at present, is dead carbon. Accordingly, the studied rocks are believed to have lost their hydrocarbon producing capabilities, even though their TOC is higher than the accepted minimum (0.4 wt. %) for source rocks under appropriate conditions. High inorganic carbon content was also observed in Utica Shale samples, which is likely resulted from high concentrations of calcite ($CaCO_3$) in this shale-gas play as indicated by Elgmati et al. (2011).

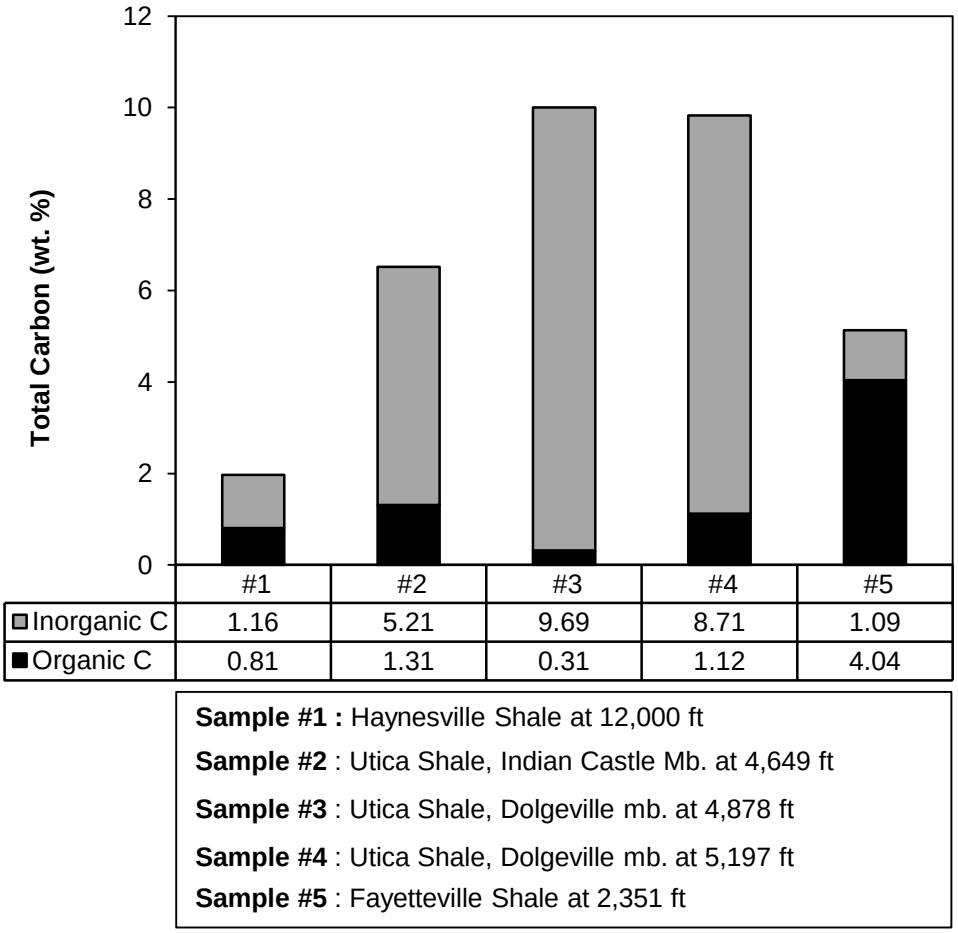

Figure 4.7. TOC Analysis Results
Measured Total Carbon (Inorganic and Organic) from the Studied Shale Gas Source Rock Samples

5. CONCLUSIONS AND RECOMMENDATIONS

5.1. CONCLUSIONS

This study supports the following conclusions:

- Submicron pore networking and rock tightness greatly affect MICP results. The Haynesville shale sample exhibited extremely low matrix permeability with a pore size of 2−20 nm; however, fractures with large openings could dominate gas transportation. The Utica shale sample offered better matrix permeability, with a pore throat size of 20−200 nm.
- A robust, detailed sequential milling and imaging procedure using SEM-FIB proved successful. SEM images showed many porous bodies that could be favorable candidates for gas storage. Various types of porosities (e.g., interparticular, intergranular, kerogen, vuggy, pyrite framboids, and fractures) were observed. Pores of organic matter were found in nano-sizes occupying 40−50% of the kerogen body.
- The reconstructed three-dimensional pore model of Fayetteville shale gas sample provided numerous petrophysical properties such as pore size distribution, porosity, tortuosity and anisotropy.
- The organic matter of Fayetteville shale has abundance of nano pores with size of 5−100 nm.
- XRD analysis provided insight into clay and nonclay mineralogy. It showed high illite content in the Haynesville and Utica shale samples. It also suggested high calcium carbonate (lime) content in the Utica shale samples.
- Calcite content proved the dominant factor increasing the shale gas contact angle and changing the wettability of shale gas rock to oil-wet. Organic matter content governed the wettability alterations of calcareous samples.
- Kerogen type IV (inert material) was identified from all the studied samples, although they differ in the percentages of individual kerogen components. The examined samples (except sample #3 from Utica Shale) likely initially contained kerogen type III (gas prone material) that transformed into type IV during the process of thermal over maturation.

- The observed palynomorphs in the palynomorph productive samples implied high level of maturation (i.e. post-mature source rocks), which denotes that the organic matter have already generated the hydrocarbons respective to their kerogen type. This signifies that the shale gas sample from Dolgeville member at the depth of 4,878 ft (inert kerogen material) has generated little dry gas, or nothing, while those of other samples (with initial kerogen type III content) have generated wet gas and condensate. Since all the samples currently contain thermally post-mature type IV kerogen, their source potential is limited to minor amounts of dry gas, or barren, at the present time.
- Measured TOC content ranged from 0.31−4.04 wt. % in the studied samples. It is likely that they once contained more TOC content that has decreased over time through the process of thermal maturation and hydrocarbon generation and expulsion.
- Good agreement between the computed TOC from the 2D SEM image and the measured TOC in the laboratory with an approximate error of 3%. This encourages exploiting 3D submicron porosimetry and kerogen content for future studies.

5.2. RECOMMENDATIONS

- The 3D submicron pore model reconstruction procedure developed for Fayetteville shale needs to be tested in other shale gas plays. If it is observed to work in other shale gas plays as well then a standard procedure for 3D SEM porosimetry in shales will be develop.
- To have a robust correlation between the organic matter maturation and kerogen porosity, it is needed to perform more intensive investigations on many shale rocks with variety of TOC values.
- In order to make submicron-scale pore imaging results universal, it is important to conduct a comprehensive statistical study at various positions along the studied section.
- Gas adsorption tests are required for better quantitative gas storativity correlation with total organic carbon content.

- The impact of clay mineralogy and total organic carbon content on shale gas wettability alteration is not well-understood. It is highly recommended to produce a correlation between the interfacial tension (IFT) and the contact angles with respect to their fluid-rock chemical compositions.

BIBLIOGRAPHY

Aguilera, R.F., Harding, T., Krause, F., and Aguilera R.: "Natural Gas Production from Tight Gas Formations: A Global Perspective," presented at the 19th World Petroleum Congress held in Madrid, Spain on June 29-July 3, 2008.

Aguilera R.: "Flow Units: From Conventional to Tight Gas to Shale Gas Reservoirs," Paper SPE 132845 presented at the Trinidad and Tobago Energy Resources Conference, Port of Spain, Trinidad, 27-30 June, 2010.

Ambrose, R. J., Hartman, R. C., Diaz-Campos, M., Akkutlu, I. Y., and Sondergeld, C. H.: "New Pore-scale Considerations for Shale Gas-in-place Calculations," SPE 131772, paper presented at the Unconventional Gas Conference, SPE, Pittsburgh, PA, February 23-25, 2010.

Amyx, J.W., Bass, D.M., Jr., and Whiting, R.L.: "Petroleum Reservoir Engineering: Physical Properties," New York City: McGraw-Hill Book Co., 1960.

Batten, D.J.: "Use of Transmitted Light Microscopy of Sedimentary Organic Matter for Evaluation of Hydrocarbon Source Potential," Proc., 4th International Palynological Conference, Lucknow, India, pp. 589-594, 1980.

Berman, A.: "The Haynesville Shale Sizzles with the Barnett Cools," World Oil Magazine. v 229, no 9, September 2008.

Biscaye, P.E.: "Mineralogy and Sedimentation of Recent Deep-sea Clay in the Atlantic Ocean and Adjacent Seas and Oceans," Geological Society of America, Bulletin 76: pp. 803-832, 1965.

Boughal, K.: "Unconventional Plays Grow in Number After Barnett Shale Blazed the Way," World Oil Magazine. v 229, no 8., August 2008.

Brooks, J.: "Organic Maturation of Sedimentary Organic Matter and Petroleum Exploration: A Review. In Organic Maturation Studies and Fossil Fuel Exploration," ed. J. Brooks. 1–38. London: Academic Press., 1981.

Carvalho, B. M.: "Paleoenvironmental Reconstruction Based on Palynological and Palynofacies Analyses of the Aptian-Albian Succession in the Sergipe Basin," Northeastern Brazil, Ruprecht-Karls-Univ., Heidelberg., 2001.

Chalmers, G., Bustin, R. M., and Powers, I.: "A Pore by Any Other Name Would Be as Small: The Importance of Meso- and Microporosity in Shale Gas Capacity," Presented at the American Association of Petroleum Geologists Annual Convention and Exhibition, Denver, CO, June 7-10, 2009.

Civan, F.: "Reservoir Formation Damage: Fundamentals, Modeling, Assessment and Mitigation," Houston, Texas: Gulf Publishing Co., 2000.

Combaz, A.: "Les Palynofacies," Rev. Micropal., v. 7, pp. 205-218., 1964.

Curtis, M.E., Ambrose, R. J., Sondergeld, C.H., and Rai, C. S.: "Structural Characterization of Gas Shales on the Micro- and Nano-Scales," Paper SPE 137693 presented at the Canadian Unconventional Resources & International Petroleum Conference, Calgary, Alberta, Canada, 19-21 October, 2010.

El Beialy, S.Y., El Atfy, H.S., Zavada, M.S., El Khoriby, E.M., and Abu-Zied, R.H.: "Palynological, Palynofacies, Paleoenvironmental and Organic Geochemical Studies on the Upper Cretaceous Succession of the GPTSW-7 Well," North Western Desert, Egypt. Marine and Petroleum Geology 27: pp. 370-385, 2010.

Elgmati, M., Zobaa, M., Zhang, H., Bai, B., and Oboh-Ikuenobe, F.: "Palynofacies Analysis and Submicron Pore Modeling of Shale-Gas Plays," Paper SPE 144267 presented at North American Unconventional Gas Conference and Exhibition, The Woodlands, TX, USA, 12-16 June, 2011.

Frantz, J.K., and Jochen, V.: "Shale Gas White Paper," Schlumberger Marketing Communications, Modified, 05-OF299, October 2005.

Ghosh, S.K., Urschel, S.F., and Friedman, G.M.: "Substitution of Simulated Well-Cuttings for Core Plugs in the Petrophysical Analysis of Dolostones: Permain San Andres Formation, Texas. Carbonates and Evaporities 2: pp. 95-100, 1987.

Grim, R.E.: "Clay Mineralogy," 2nd Edition. McGraw-Hill, New York, 596 pp., 1968.

Hayden, J., and Pursell, D.: "The Barnett Shale: Visitor"s Guide to the Hottest Gas Play in the US," Pickering Energy Partners, Inc., October 2005.

Hillwood International Energy: "Fayetteville Shale Power," Arkansas, USA, July 12, 2007.

Ibrahim, M. I. A., Abul Ela, N. M., and Kholeif, S. E.: "Paleoecology, Palynofacies, Thermal Maturation and Hydrocarbon Source-Rock Potential of the Jurassic-Lower Cretaceous Sequence in the Subsurface of the North Eastern Desert," Egypt. Qatar Univ., Sci. J., v. 17 (1), pp. 153-172, 1997.

Jarvie D.M.: "Total Organic Carbon (TOC) Analysis in Treatise of Petroleum Geology," Handbook of Petroleum Geology, Source and Migration Processes and Evaluation Techniques, Ed. R.K.Merrill, AAPG Press., Tulsa, OK, 1991.

Jarvie D.M.: "Evaluation of Hydrocarbon Generation and Storage in Barnett Shale, Ft. Worth Basin, Texas," Humble Geochemical Services Presentation, 2004.

Jarvie, D.M., Hill, R.J., Ruble, T.E., and Pollastro, R.M.: "Unconventional Shale-Gas Systems: The Mississippian Barnett Shale of North-Central Texas as One Model for Thermogenic Shale-Gas Assessment," AAPG Bulletin 91: pp. 475-499, 2007.

Johnston, J., III, Heinrich, P., Lovelace, J., McCulloh, R., and Zimmerman. R.: "Stratigraphic Charts of Louisiana," Louisiana Geological Survey. Folio series no. 8, 2000.

Jones, N.: "X-ray Mineralogy and the X-ray Diffractometer," Oshkosh, Wisconsin: University of Wisconsin Oshkosh, 1996.

Kale S.: "Petrophysical Characterization of Barnett Shale Play," Masters Thesis, Oklahoma U., Norman, Oklahoma, 2009.

Kale, S., Rai, C.S., and Sondergeld, C. H.: "Rock Typing in Gas Shales," Paper SPE 134539 presented at the SPE Annual Technical Conference and Exhibition, Florence, Italy, 19-22 September, 2010.

Kopaska-Merkel, D.C., and Amthor, J.E.: "Very High-Pressure Mercury Porosimetry as a Tool in Reservoir Characterization," Carbonates and Evaporites 3: pp. 53-63, 1988.

Leverett, M.C.: "Capillary Behavior in Porous Solids," Trans. AIME 142: pp. 152-169, 1941.

Leverson, A. L.: "Geology of Petroleum," 2001 Edition: Tulsa, AAPG Foundation, 724 pp., 1954.

Loucks, R. G., Reed, R.M., Ruppel, S. C., and Jarvie, D.M.: "Morphology, Genesis, and Distribution of Nanometer-Scale Pores in Siliceous Mudstones of the Mississippian Barnett Shale," Journal of Sedimentary Research 79: pp. 848-861, 2009.

Masters, J.A. and Gray, J.K.: "Resources Pyramid," Canadian Hunter, Calgary, Canada, crica, 1980.

Moore, D.M., and Reynolds, R.C. Jr.: "X-Ray Diffraction and the Identification and Analysis of Clay Minerals," New York City: Oxford University Press, 1989.

Murray, H.H.: "Applied Clay Mineralogy: Occurrences, Processing and Application of Kaolins, Bentonites, Palygorskite- Sepiolite, and Common Clays," The Netherlands: Elsevier, 2007.

"North American Natural Gas Supply Assessment," Prepared for American Clean Skies Foundation, Navigant Consulting, July 4, 2008.

Oehler, J. H.: "Using Geothermal Gradient to Estimate Source Rock Quality," Unpublished Course Notes, 1983.

Perrodon, A.: "Dynamics of Oil and Gas Accumulation," Elf Aquitaine, 368 pp., 1983.

Peters, K.E., Cassa, M.R.: "Applied Source Rock Geochemistry," In The Petroleum System—From Source to Trap, ed. L.B. Magoon, and W.G. Dow. AAPG Memoir 60: pp. 93-120, 1994.

Sharma, M.: "Formation Damage-Maximizing the Productivity of Oil And Gas Wells," Unpublished Course Notes, Vienna, Austria, June 26-30, 2006.

Sliwinski, J., Harrington, J., Power, M., Hughes, P., and Yeung, B.: "A High Definition Mineralogical Examination of Potential Gas Shales," AAPG 2010, New Orleans (11-14 April 2010), Abstract Volume, 239 pp.

Sondergeld, C. H., Ambrose, R. J., Rai, C. S., and Moncrieff, J.: "Micro-Structural Studies of Gas Shales," Paper SPE 131771 presented at the Unconventional Gas Conference, Pittsburgh, PA, USA, 23-25 February, 2010.

Sumi, L.: "Shale Gas: Focus on the Marcellus Shale," Oil and Gas Accountability Project (OGAP), May 2008.

Tiab, D., and Donaldson, E.: "Petrophysics: Theory and Practice of Measuring Reservoir Rock and Fluid Transport Properties," Houston, TX: Gulf Publishing Co., 1996.

Tissot B.P.: "Recent Advances in Petroleum Geochemistry Applied to Hydrocarbon Exploration," AAPG Bulletin, V.68(5): pp. 545-563, 1984.

Tomutsa, L., Silin, D., and Radmilovic, V.: "Analysis of Chalk Petrophysical Properties By Means of Submicron-Scale Pore Imaging and Modeling," SPEREE 10(3): pp. 285-293, SPE 99558, 2007.

Traverse, A.: "Paleopalynology," Dordrecht: Springer, 2007.

Tyson, R. V.: "Sedimentary Organic Matter: Organic Facies and Palynofacies," Chapman and Hall, London, 615 pp., 1995.

Tyson, R. V.: Palynofacies Analysis. In *Applied Micropalaeontology*, Kluwer Academic Publishers, pp. 153-191, 1993.

U.S. Department of Energy: "Modern Shale Gas Development in the United States: A Primer," Ground Water Protection Council, Oklahoma City, OK, April 2009.

"U.S. Shale Gas: An Unconventional Resource," Unconventional Challenges, Halliburton Energy Services, 2008.

Wang, F. P., and Reed, R. M.: "Pore Networks and Fluid Flow in Gas Shales," SPE 124253, paper presented at the Annual Technical Conference and Exhibition, SPE, New Orleans, LA, October 4-7, 2009.

Wardlaw, N.C., and Taylor, R.P.: "Mercury Capillary Pressure Curves and the Interpretation of Pore Structure and Capillary Behavior in Reservoir Rocks," Bulletin of Canadian Petroleum Geology 24(2): pp. 225-262, 1976.

Wyllie, M.R.J., and Gardner, G.H.F.: "The Generalized Kozeny-Carman Equation," World Oil 146(4): pp. 121-128, 1958.

Yaalon, D.H.: "Mineral Composition of Average Shale," Clay Mineral Bulletin 5(27): pp. 31-36, 1962.

Zobaa, M.K., Oboh-Ikuenobe, F.E., Zavada, M.S.: "Applications of Palynology for Hydrocarbon Exploration: Case Studies from Egypt, Eastern Tennessee (USA) and the Gulf of Mexico," AAPG Annual Convention and Exhibition, Abstract, Denver, Colorado, USA, 7-10 June, 2009.

Zobaa, M.K., Zavada, M.S., Whitelaw, M.J.: "Palynofacies Analysis, Source Rock Evaluation and Organic Thermal Maturation of the Gray Fossil Site," Gray, Tennessee. AAPG Eastern Section Meeting, Lexington, Kentucky, USA, 16-18 September, 2007.

Zobaa, M.K.: "Subsurface Jurassic-Cretaceous Applied Palynology of the Sharib-1X and Ghoroud-1X wells, North Western Desert, Egypt," Masters Thesis, Benha University, Egypt, 2006.

VITA

Malek Elgmati was born September 16, 1982 in Tripoli, Libya. He received his Bachelor of Science degree in Petroleum Engineering from Alfateh University at Tripoli, Libya in 2005. He worked as a Consultant Reservoir Engineer with Schlumberger Oilfield Services in Libya for two years in the Data and Consulting Services (DCS) department. He has also served as a Teaching Assistant in the Department of Geological Sciences and Engineering at Missouri University of Science and Technology for one and half year. Recently, he co-authored three SPE papers about shale gas submicron pore tomography, palynofacies analysis and average reservoir pressure estimation from flow after flow testing. In May 2011, he will receive his Masters in Petroleum Engineering from Missouri University of Science and Technology at Rolla, Missouri.